Hindawi
Shock and Vibration
Volume 2019, Article ID 2542349, 21 pages
https://doi.org/10.1155/2019/2542349

Research Article

Fourier Series Approach for the Vibration of Euler–Bernoulli Beam under Moving Distributed Force: Application to Train Gust

Shupeng Wang,[1] **Weigang Zhao**,[2] **Guangyuan Zhang**,[2] **Feng Li**,[1] **and Yanliang Du**[2]

[1]*School of Civil Engineering, Wuhan University, Wuhan 430072, China*
[2]*Structural Health Monitoring and Control Institute, Shijiazhuang Tiedao University, Shijiazhuang 050043, China*

Correspondence should be addressed to Shupeng Wang; shupeng2hao@163.com

Received 30 August 2019; Revised 28 October 2019; Accepted 1 November 2019; Published 26 November 2019

Academic Editor: Pedro Museros

The dynamic response of an Euler–Bernoulli beam under moving distributed force is studied. By decomposing the distributed force into Fourier series and extending them to semi-infinite sine waves, the complex procedure for solving this problem is simplified to three base models, which are calculated by the modal superposition method further. The method is proved to be highly accurate and computational efficient by comparing with the finite element method. For verifying the theory and exploring the relationship between dynamic pressure due to train gust and vibration of the structure, a site test was conducted on a platform canopy located on the Beijing-Shanghai high-speed railway in China. The results show the theory can be used to evaluate the dynamic response of the beam structure along the trackside due to the train gust. The dynamic behavior of a 4-span continuous steel purlin is studied when the structure is subjected to the moving pressure due to different high-speed train passing.

1. Introduction

Moving load dynamic problem of the beam structure is a classical mechanical problem, which may be traced back to the mid-19th century. In the construction of railway, there was no agreement among engineers over the effect of a moving load on the bridge. Researchers such as Prof Willis, Stokes, and Homersham Cox did a lot of investigations in the early years. This history was chronicled by Timoshenko [1]. As the easiest case, the bridge was modeled as a simply supported beam, traversed by a moving force with constant speed [2]. It was found that the dynamic response of the beam was related with the speed of force, and the maximum dynamic deflection can be 1.74 times as high as the static deflection for the simply supported beam [3, 4]. Meanwhile, it was shown that the dynamic response of the beam would achieve an extreme small value at a certain speed. This phenomenon was called cancellation [5]. Around this problem, numerous researchers have made great endeavor on it (see, e.g., [6–12]). The theoretical progress and development history have been intensively reviewed (see, e.g., [13]).

However, the moving load problem of the beam structure is still an active topic in structural dynamics even though it has been studied over a century. There are two reasons for this. The first one is about the model of the moving load from vehicle, which has been developed from the force-beam interaction model to the vehicle (mass)-beam interaction model. The force-beam interaction model is a classical model, in which the beam is subjected to one or a series of moving concentrated force [2, 6]. In Frýba's monograph [14], many problems around this load model have been extensively discussed. The vehicle-beam interaction model is more precise by considering the traveling vehicle as moving masses [15, 16] or sprung masses for the contribution of the vehicle suspension system [17, 18]. With the development of transportation, new problems arise, for example, moving distributed force problem due to high-speed train gust, which will be studied in this paper. The second reason is about the calculation method for solving this problem. Numerous methods have been proposed to evaluate the moving load problem (see, e.g., [19–30]). However, one fact we need to face is that until now, the applications of these methods are limited to special moving load problems.

From mathematical aspect, the moving distributed force can be described as a function of space moving at a certain

speed, which is more complex than the two previous load models in which a Dirac delta function defines the concentrated load. From physical aspect, there are more parameters (e.g., the length of beam, the length of load, and the distributed form of load) need to be considered. Besides, the whole procedure of the load passing by the beam may be divided into four stages, such as arrival of load, whole load acting on the beam, departure of load, and free vibration of the beam after load leaving. All these factors make the moving distributed force problem more complex than the concentrated load case. It should be noted that a simple case of moving distributed force problem has been studied by Esmailzadeh and Ghorashi [31, 32] in the early years. In their studies, a bridge was assumed to be a simply supported beam and a traveling train was assumed to be a segment of uniform distributed force moving on the beam. Frýba [14] has deduced a stationary solution for the simply supported beam subjected to a moving endless strip of uniform distributed load. Considering the effect of track structure, the moving axle loads of the train were modeled as a sequence of block-distributed loads by Museros et al. [33], and the influence of shapes of load distribution on bridge vibration was studied by Rehnström and Daniel [34]. Erik et al. [35] gave a detailed analysis about the effect of axle load spreading. The reduction effect of the track structure was investigated analytically by Jin et al. [36]. Both arrival and departure of load were neglected in all these studies.

The purpose of this study is to develop a general method for solving the dynamic response of a beam subjected to moving distributed force. By using this method, vibration of the beam under moving pressure due to high-speed train gust is investigated. The remainder of this paper is organized as follows: Section 2 presents a general model. Section 3 gives the solution and some parametric discussion. The accuracy and computational efficiency of the suggested method is verified in this section. Based on the general model, the vibration of multispan continuous beam under moving distributed load is analyzed in Section 4. Section 5 shows the distributed form of train gust and its Fourier series representation. Some characters of the dynamic pressure from the site test under a platform canopy are analyzed in this section. Section 6 presents numerical results. By comparing the results from calculation and site test, the general method is verified. The dynamic behaviors of a 4-span continuous steel purlin under different high-speed train passing are studied. Section 7 gives a conclusion of the study.

2. General Model

Firstly, we introduce a general model, in which a single-span Euler–Bernoulli beam with general boundary condition is subjected to a moving distributed force, as shown in Figure 1. Two axial coordinates are introduced: the global coordinate x for the whole system which is the distance from the left support of the beam in the direction of motion, and the local coordinate $\tilde{x}$ for the force that moves with the distributed force. The relationship between the two coordinates is

$$x = \tilde{x} + vt - \tilde{L}, \tag{1}$$

where $\tilde{L}$ is the length of the distributed force, v is the speed of the distributed force, and t is the time.

The general equation of motion of a single-span Euler–Bernoulli beam under a moving distributed force can be expressed as

$$EI\frac{\partial^4 u(x,t)}{\partial x^4} + \overline{m}\frac{\partial^2 u(x,t)}{\partial t^2} + c\frac{\partial u(x,t)}{\partial t} = f, \tag{2}$$

where E is the Young's modulus of material, I is the moment of inertia of the beam-section, $u(x,t)$ is the transverse deflection of the beam at point x and time t, $\overline{m}$ is the mass per unit length, and c is the damping constant. L is the length of the beam and f is the moving distributed force, which can be written in the local coordinate as

$$f = f(\tilde{x})[H(\tilde{x}) - H(\tilde{x} - \tilde{L})], \tag{3}$$

in which $H(\tilde{x})$ is the Heaviside unit function defined as follows:

$$H(\tilde{x}) = \begin{cases} 0, & \tilde{x} < 0, \\ 1, & \tilde{x} \geq 0. \end{cases} \tag{4}$$

Considering the Fourier series expansion of $f(\tilde{x})$ and the relationship between the two coordinates, equation (3) can be reexpressed as

$$f = f_1 + \sum_{n=1}^{\infty}(f_{2n} + f_{3n}), \tag{5}$$

where f_1, f_{2n}, and f_{3n} are the Fourier series representations of the distributed force given as follows:

$$f_1 = \tilde{f}_1(x,t) - \tilde{f}_1\left(x, t - \frac{\tilde{L}}{v}\right), \tag{6a}$$

$$f_{2n} = \tilde{f}_{2n}(x,t) - \tilde{f}_{2n}\left(x, t - \frac{\tilde{L}}{v}\right), \tag{6b}$$

$$f_{3n} = \tilde{f}_{3n}(x,t) - \tilde{f}_{3n}\left(x, t - \frac{\tilde{L}}{v}\right), \tag{6c}$$

$$\tilde{f}_1(x,t) = a_0[1 - H(x - vt)], \tag{7a}$$

$$\tilde{f}_{2n}(x,t) = a_n \cos\left[\frac{2\pi n(x - vt)}{\tilde{L}}\right][1 - H(x - vt)], \tag{7b}$$

$$\tilde{f}_{3n}(x,t) = b_n \sin\left[\frac{2\pi n(x - vt)}{\tilde{L}}\right][1 - H(x - vt)], \tag{7c}$$

in which a_0, a_n, and b_n are the Fourier series coefficients:

$$a_0 = \frac{1}{\tilde{L}}\int_0^{\tilde{L}} f(\tilde{x})\mathrm{d}\tilde{x}, \tag{8a}$$

$$a_n = \frac{2}{\tilde{L}}\int_0^{\tilde{L}} f(\tilde{x})\cos\left(\frac{2\pi n\tilde{x}}{\tilde{L}}\right)\mathrm{d}\tilde{x}, \tag{8b}$$

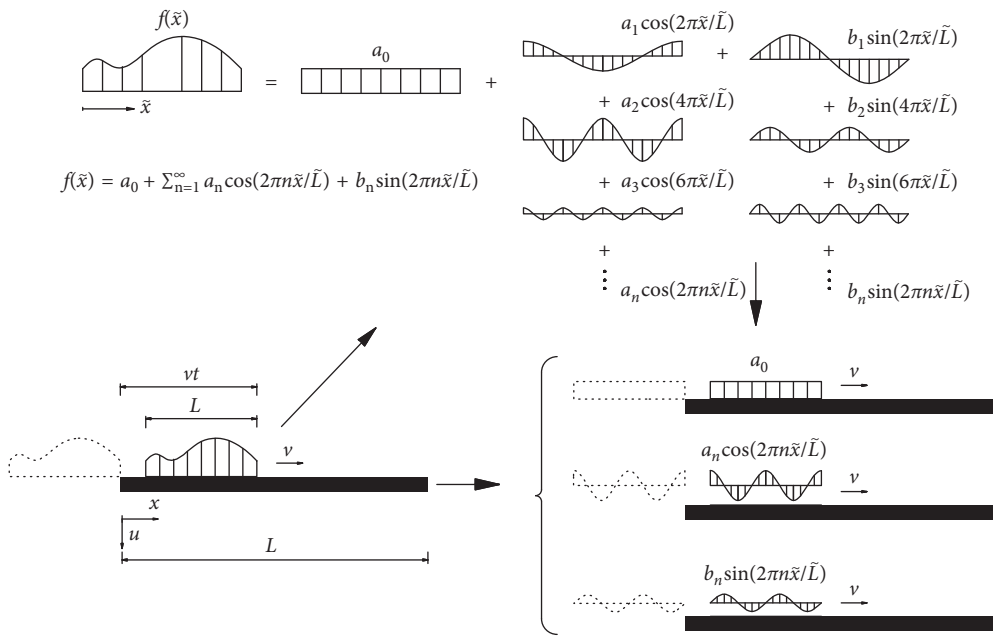

Figure 1: A single-span beam subjected to a moving distributed force and its equivalent model.

$$b_n = \frac{2}{\tilde{L}}\int_0^{\tilde{L}} f(\tilde{x})\sin\left(\frac{2\pi n\tilde{x}}{\tilde{L}}\right)\mathrm{d}\tilde{x}. \tag{8c}$$

According to the attributes of linear system, the solution of equation (2) can be expressed as

$$\begin{aligned} u(x,t) &= u_1(x,t) + \sum_{n=1}^{\infty}\left[u_{2n}(x,t) + u_{3n}(x,t)\right] \\ &= \tilde{u}_1(x,t) - \tilde{u}_1\left(x, t - \frac{\tilde{L}}{v}\right) + \sum_{n=1}^{\infty}\left[\tilde{u}_{2n}(x,t)\right. \\ &\quad \left. - \tilde{u}_{2n}\left(x, t - \frac{\tilde{L}}{v}\right)\right] + \sum_{n=1}^{\infty}\left[\tilde{u}_{3n}(x,t) - \tilde{u}_{3n}\left(x, t - \frac{\tilde{L}}{v}\right)\right], \end{aligned} \tag{9}$$

where u_1, u_{2n}, and u_{3n} are the transverse deflections of beam under f_1, f_{2n}, and f_{3n}. $\tilde{u}_1$, $\tilde{u}_{2n}$, and $\tilde{u}_{3n}$ can be solved by

$$EI\frac{\partial^4\tilde{u}_1(x,t)}{\partial x^4} + \overline{m}\frac{\partial^2\tilde{u}_1(x,t)}{\partial t^2} + c\frac{\partial\tilde{u}_1(x,t)}{\partial t} = \tilde{f}_1(x,t), \tag{10a}$$

$$EI\frac{\partial^4\tilde{u}_{2n}(x,t)}{\partial x^4} + \overline{m}\frac{\partial^2\tilde{u}_{2n}(x,t)}{\partial t^2} + c\frac{\partial\tilde{u}_{2n}(x,t)}{\partial t} = \tilde{f}_{2n}(x,t), \tag{10b}$$

$$EI\frac{\partial^4\tilde{u}_{3n}(x,t)}{\partial x^4} + \overline{m}\frac{\partial^2\tilde{u}_{3n}(x,t)}{\partial t^2} + c\frac{\partial\tilde{u}_{3n}(x,t)}{\partial t} = \tilde{f}_{3n}(x,t). \tag{10c}$$

In fact, equation (10a) is the general equation of motion of the beam under a strip of endless uniform distributed force moving at constant speed v; equations (10b) and (10c) are the general equations of motion of the beam under a strip of endless sinusoidal distributed force moving at constant speed v. The three problems will be called base models in the following sections, as shown in Figure 2.

3. Solution and Discussion

3.1. Solution of the General Model. According to the modal superposition method, the transverse displacements $\tilde{u}_1(x,t)$, $\tilde{u}_{2n}(x,t)$, and $\tilde{u}_{3n}(x,t)$ can be written in the modal coordinates as

$$\tilde{u}_1(x,t) = \sum_{m=1}^{\infty}\phi_m(\xi_m, x)\tilde{q}_{1m}(t), \tag{11a}$$

$$\tilde{u}_{2n}(x,t) = \sum_{m=1}^{\infty}\phi_m(\xi_m, x)\tilde{q}_{2nm}(t), \tag{11b}$$

$$\tilde{u}_{3n}(x,t) = \sum_{m=1}^{\infty}\phi_m(\xi_m, x)\tilde{q}_{3nm}(t), \tag{11c}$$

where $\tilde{q}_{1m}$, $\tilde{q}_{2nm}$, and $\tilde{q}_{3nm}$ are the mth modal coordinates of the base models for equations (11a), (11b), and (11c), respectively, and $\phi_m(\xi_m, x)$ is the mth mode shape of the beam given as follows:

$$\begin{aligned} \phi_m(\xi_m, x) &= A_m\sin(\xi_m x) + B_m\cos(\xi_m x) + C_m\sinh(\xi_m x) \\ &\quad + D_m\cosh(\xi_m x), \end{aligned} \tag{12}$$

in which A_m, B_m, C_m, and D_m are the coefficients of the mth mode shape and ξ_m is the mth eigenvalue of the beam. All these parameters can be solved by the boundary conditions of the beam. It should be pointed out that ξ_m is a function of the length of beam, and $\xi_m L$ is often considered to be one parameter for dimensionless

analysis. For example, the values of $\xi_m L$ of the simply supported beam are $\pi, 2\pi, \ldots, m\pi$.

By substituting equations (11a), (11b), and (11c) into equations (10a), (10b), and (10c), multiplying $\phi_k(\xi_k, x)$ to both sides, and then integrating with respect to x from 0 to L, equations (10a), (10b), and (10c) can be decomposed as

$$\frac{d^2\tilde{q}_\chi(t)}{dt^2} + 2\zeta_m\omega_m\frac{d\tilde{q}_\chi(t)}{dt} + \omega_m^2\tilde{q}_\chi(t) = p_\chi(t), \tag{13}$$

where ω_m is the mth circular frequency of beam, $\omega_m = \xi_m^2\sqrt{EI/\overline{m}}$. ζ_m is the mth damping ratio of beam, $\zeta_m = c/(2\overline{m}\omega_m)$, $\tilde{\phi}_m = \int_0^L \phi_m^2(\xi_m, x)\mathrm{d}x$. In order to save space, three equations of the base models are condensed to one, and "χ" is used to represent the subscripts "$1m$," "$2nm$," and "$3nm$." The modal force p_χ in equation (13) can be calculated as

$$p_\chi(t) = \begin{cases} \dfrac{a_0}{\overline{m}\tilde{\phi}_m\xi_m}\Gamma_\chi(t)\mathbf{A}_m, & 0 \le t \le t_1, \\ \dfrac{a_0}{\overline{m}\tilde{\phi}_m\xi_m}\Pi_\chi(t)\mathbf{A}_m, & t > t_1, \end{cases} \tag{14}$$

where $\mathbf{A}_m = [\,A_m \;\; B_m \;\; C_m \;\; D_m\,]^T$, $t_1 = L/v$, and Γ_χ and Π_χ stand for (Γ_{1m}, Γ_{2nm}, Γ_{3nm}) and (Π_{1m}, Π_{2nm}, Π_{3nm}), respectively:

$$\begin{aligned} \Gamma_{1m}(t) &= [\,1 - \cos(\alpha\lambda_m\omega_1 t) \;\; \sin(\alpha\lambda_m\omega_1 t) \;\; \cosh(\alpha\lambda_m\omega_1 t) - 1 \;\; \sinh(\alpha\lambda_m\omega_1 t)\,], \\ \Pi_{1m} &= [\,1 - \cos(\xi_m L) \;\; \sin(\xi_m L) \;\; \cosh(\xi_m L) - 1 \;\; \sinh(\xi_m L)\,], \end{aligned} \tag{15}$$

in which α is a dimensionless speed parameter which has been employed by other researchers [7, 14], $\alpha = (\xi_1 v)/\omega_1 = v/v_{\mathrm{cr}}$. v_{cr} is called the critical speed, $v_{\mathrm{cr}} = \xi_1\sqrt{EI/\overline{m}}$. λ_m is the ratio of the mth eigenvalue to the first, $\lambda_m = \xi_m/\xi_1$. Γ_{2nm}, Π_{2nm}, Γ_{3nm}, and Π_{3nm} are the four time functions, which are related with the speed parameter α and the ratio of wavenumber to the first eigenvalue Q_n, $Q_n = (2n\pi)/(\eta\xi_1 L)$. η is the length ratio of the distributed force to the beam, $\eta = \tilde{L}/L$. Due to limited space, their complex expressions are not illustrated here. More details can be referred to Appendix A.

It should be noted that equation (13) can be deemed as a single-degree-of-freedom (SDOF) system which is subjected to two kinds of impulsive force in two phases. During the second phase ($t > t_1$), the response of the beam is the sum of the free-vibration motion due to the force in the first phase and the forced vibration motion due to the force in the second phase. The modal coordinate $\tilde{q}_\chi$ can be calculated by using the Duhamel integral formulation [37] given as follows:

$$\tilde{q}_\chi(t) = \begin{cases} \dfrac{a_0}{\overline{m}\hat{\phi}_m\omega_1^2\xi_1 L}\hat{\Gamma}_\chi(t)\mathbf{A}_m, & 0 \le t \le t_1, \\ \dfrac{a_0}{\overline{m}\hat{\phi}_m\omega_1^2\xi_1 L}\breve{\Gamma}_\chi(t)\mathbf{A}_m, & t > t_1, \end{cases} \tag{16}$$

where

$$\hat{\phi}_m = \frac{\tilde{\phi}_m}{L} = \int_0^1 \phi_m^2(\xi_m L, x)\mathrm{d}x, \tag{17}$$

$\hat{\Gamma}_\chi$ and $\breve{\Gamma}_\chi$ stand for ($\hat{\Gamma}_{1m}$, $\hat{\Gamma}_{2nm}$, $\hat{\Gamma}_{3nm}$) and ($\breve{\Gamma}_{1m}$, $\breve{\Gamma}_{2nm}$, $\breve{\Gamma}_{3nm}$), respectively, which are the time functions with variables: α, η, Q_n, and β_m. β_m is a series of dimensionless damping parameter, $\beta_m = \lambda_m^2\zeta_m$. Due to limited space, their complex expressions are not illustrated here. More details can be referred to Appendixes B, C, and D.

3.2. Comparison and Parametric Discussion. A simply supported beam is considered in this section as a benchmark problem for studying the different responses of the beam under three kinds of moving load conditions. The solution accuracy and computation efficiency of the proposed Fourier series mode superposition method (denoted by FSM) are evaluated with the finite element method (denoted by FEM). It should be noted that there is no reference for solving the moving distributed load problem by using FEM until now. By some special treatment of distributed force, element size, and time step, existing FEM packages can be used to evaluate this problem. More details are shown in Appendix E. The properties of the beam are as follows: area of cross section $A = 9.808 \times 10^{-3}\,\mathrm{m}^2$, moment of inertia $I = 4.29 \times 10^{-4}\,\mathrm{m}^4$, length $L = 24\,\mathrm{m}$, Young's modulus $E = 2.06 \times 10^{11}\,\mathrm{N/m}^2$, Poisson's ratio $\nu = 0.3$, and mass density $\rho = 7850\,\mathrm{kg/m}^3$. The Fourier series coefficients a_0, a_n, and b_n are assumed to be 1 for the comparison of dynamic effects between different load conditions. The length ratio of the distributed force to the beam η, the speed parameter α, and the damping parameter β_m are assumed to be 1.3, 0.6, and 0, respectively. The speed of distributed force is calculated, with a result of 71.573 m/s. The lowest 10 mode shapes are considered in the calculation since it can give sufficient results for all the calculated cases, which have been confirmed by authors. $\overline{m}\omega_1^2$ will be neglected in the results of displacement (u_1, u_{2n}, u_{3n}) in this section for the sake of dimensionless analysis since it is a constant that does not have relationship with modes number m and Fourier series number n from equation (16). Besides, $\omega_1 t$ is deemed as one parameter for dimensionless analysis.

Figure 3 compares the central displacements of the simply supported beam under four kinds of distributed force (uniform distributed force f_1, sine form distributed force $f_{3n}(n = 1)$, and two cosine form distributed force $f_{2n}(n = 1, 3)$) by the proposed method and FEM. They all show that the dynamic responses obtained by the FEM converge gradually to the results by the proposed method as the number of elements increases. The FEM with less elements can make a good approximation of the dynamic response for the uniform distributed force f_1 and sine form

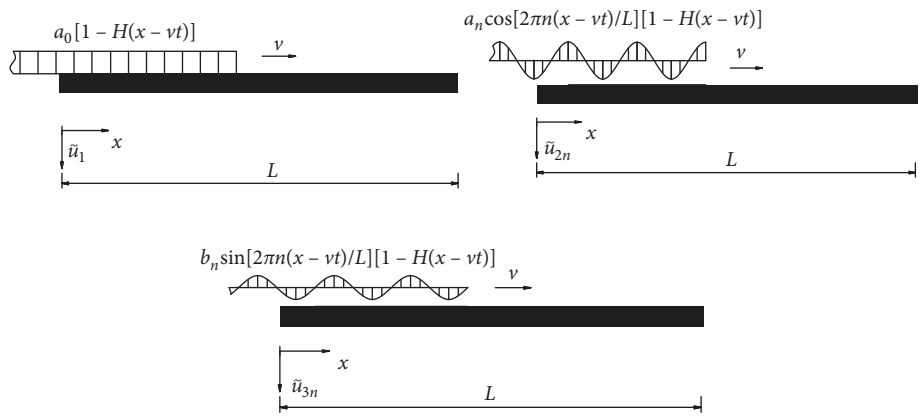

FIGURE 2: Base models of the single-span beam under moving distributed force. Beam under a strip of endless (a) uniform distributed force, (b) cosine form distributed force, and (c) sine form distributed force.

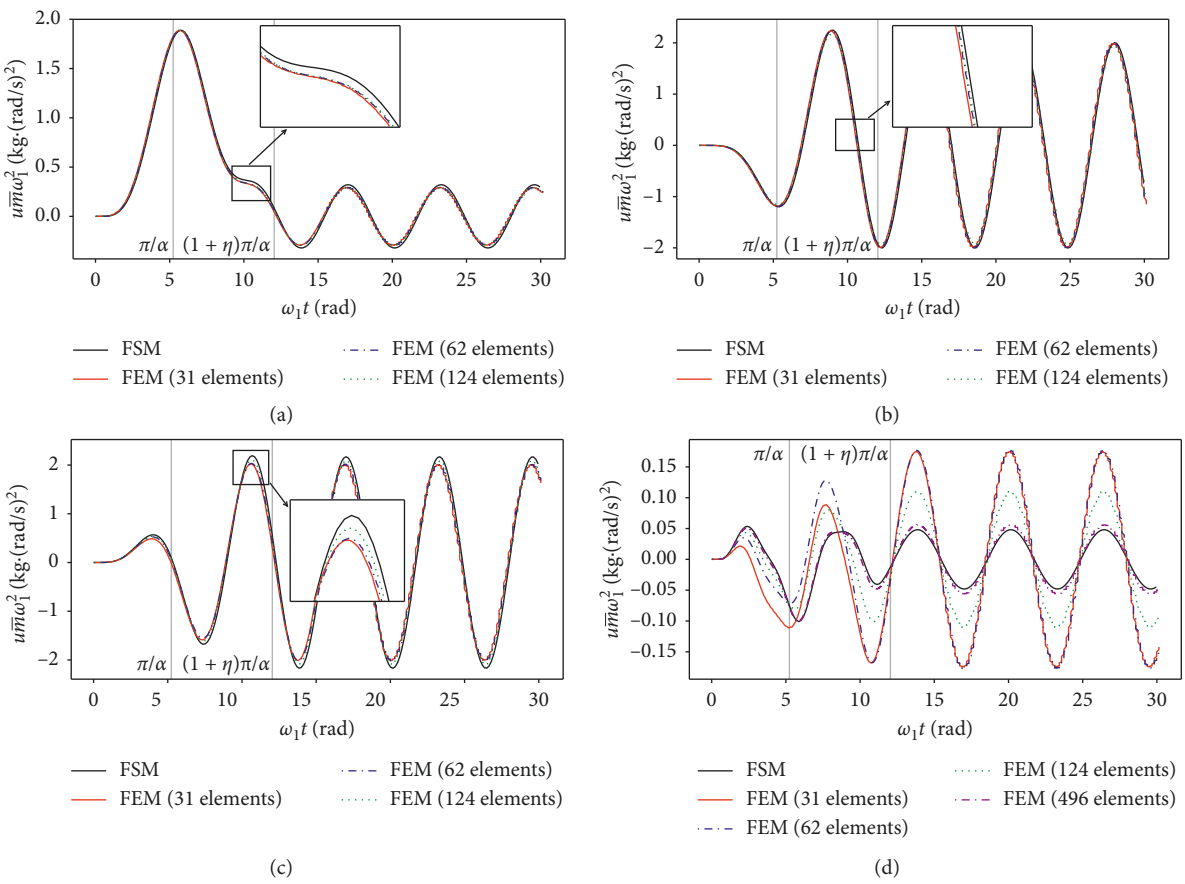

FIGURE 3: Comparisons of dynamic responses of the simply supported beam obtained by FSM and FEM ($\eta = 1.3$; $\alpha = 0.6$; $\beta_m = 0$; π/α stands for the time that the whole length of beam is subjected to the distributed force; $(1+\eta)\pi/\alpha$ stands for the time that the whole length of force have departed from the beam, which will vibrate freely later). (a) Displacement of beam u_1 due to f_1. (b) Displacement of beam u_{3n} due to f_{3n} $(n = 1)$. (c) Displacement of beam u_{2n} due to f_{2n} $(n = 1)$. (d) Displacement of beam u_{2n} due to f_{2n} $(n = 3)$.

distributed force f_{3n} $(n = 1)$, but lead some deviation for cosine form distributed force f_{3n}, especially when n is large. The computation times were about 0.16 s for FSM and 64 s, 125 s, 252 s, and 1250 s for FEM with 31, 62, 124, and 496 elements, respectively. The proposed method was programed with PYTHON, and the FEM results were calculated by the commercial FEM package ANSYS 16.0. They all were conducted on a desktop PC with Intel Core i5-6440HQ processor and 8 GB of DDR3 memory.

Figure 4 shows the comparisons of dynamic responses of the simply supported beam under different distributed force, but with the same Fourier Series number n. The maximum

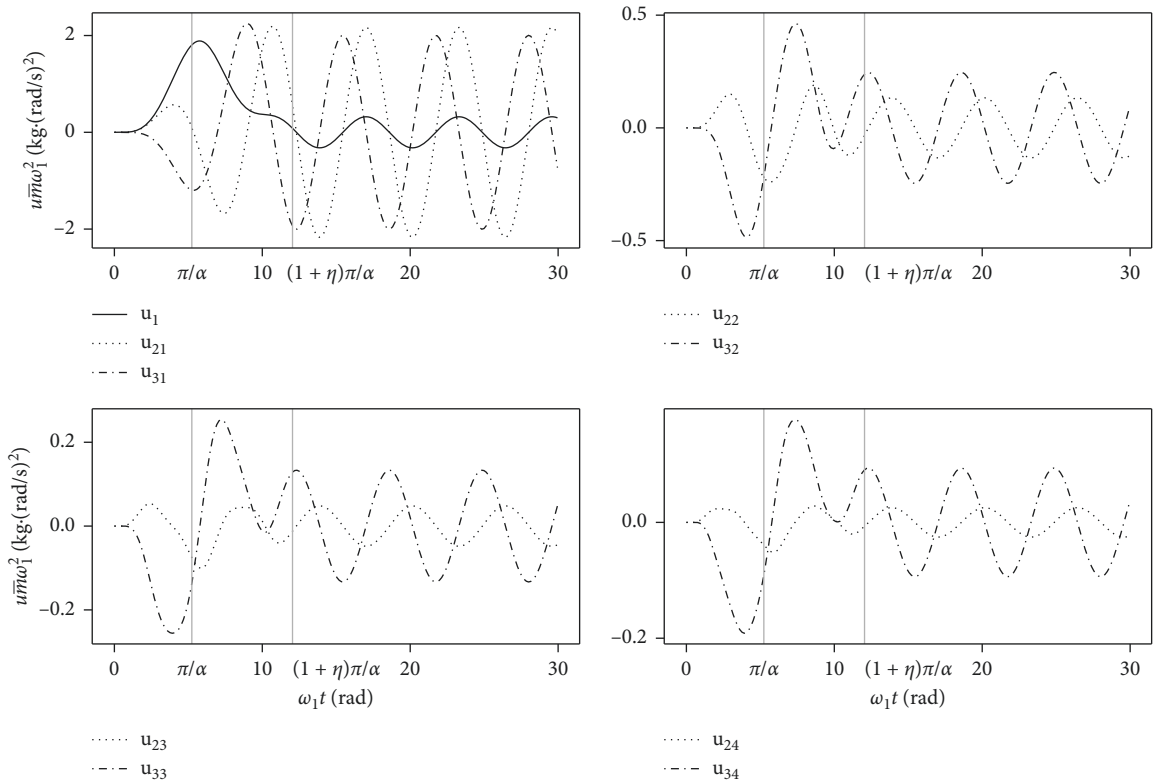

Figure 4: Comparisons of dynamic responses of the simply supported beam under different distributed force.

dynamic responses of the simply supported beam happen during the forced vibration stage for all these force conditions. When the Fourier series number n is 1, the values of the maximum displacement of the simply supported beam under sine and cosine form distributed force are closed, which are larger than the value under uniform distributed force. When n is larger than 1, the response of the beam under sine form distributed force is larger than that of the beam under cosine form distributed force. The responses of the beam under the both kinds of force are decreasing as n increases.

The influence of the length ratio η to the response of beam is shown in Figure 5. The speed parameter α, the damping parameter β_m, and the Fourier series number n are assumed to be 0.6, 0, and 1, respectively. The length ratio of the distributed force to the beam η is from 0.25 to 2. The maximum displacements of the beam under different length distributed force are shown in Figure 5. There are three intersections between the three curves. When η is less than 1.06, the value of $\max(u_1\overline{m}\omega_1^2)$ is larger than the values of $\max(u_{21}\overline{m}\omega_1^2)$ and $\max(u_{31}\overline{m}\omega_1^2)$. When η is larger than 1.17, the values of $\max(u_{21}\overline{m}\omega_1^2)$ and $\max(u_{31}\overline{m}\omega_1^2)$ both exceed the value of $\max(u_1\overline{m}\omega_1^2)$. When η is less than 1.35, $\max(u_{31}\overline{m}\omega_1^2)$ is larger than $\max(u_{21}\overline{m}\omega_1^2)$, and vice versa. The $\max(u_{21}\overline{m}\omega_1^2)$ curve achieves a maximum value 2.61 at $\eta = 1.67$, and $\max(u_{31}\overline{m}\omega_1^2)$ curve achieves a maximum value 2.40 at $\eta = 1.52$.

The influence of the speed parameter α to the response of the beam is shown in Figure 6. The length ratio η, the damping parameter β_m, and the Fourier series number n are

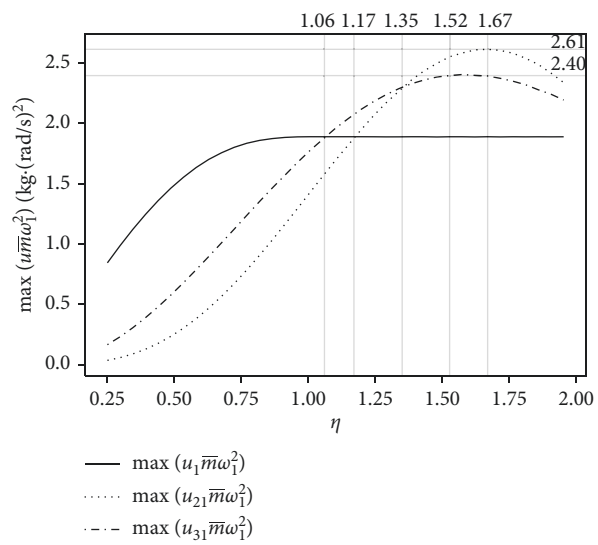

Figure 5: The maximum displacement curves of the beam under three kinds of moving load conditions with different length ratios η ($n = 1$; $\alpha = 0.6$; $\beta_m = 0$; η is from 0.25 to 2).

assumed to be 1.3, 0, and 1, respectively. The speed parameter α is from 0 to 2. There are the phenomena of maximum dynamic response and cancellation when the three kinds of distributed force pass on the beam. $\max(u_1\overline{m}\omega_1^2)$, $\max(u_{21}\overline{m}\omega_1^2)$, and $\max(u_{31}\overline{m}\omega_1^2)$ achieve maximum values 2.32, 2.20, and 2.36 when α is equal to 1.21, 0.63, and 0.71, respectively. When α is less than 0.6, the values of $\max(u_{21}\overline{m}\omega_1^2)$ and $\max(u_{31}\overline{m}\omega_1^2)$ are closed.

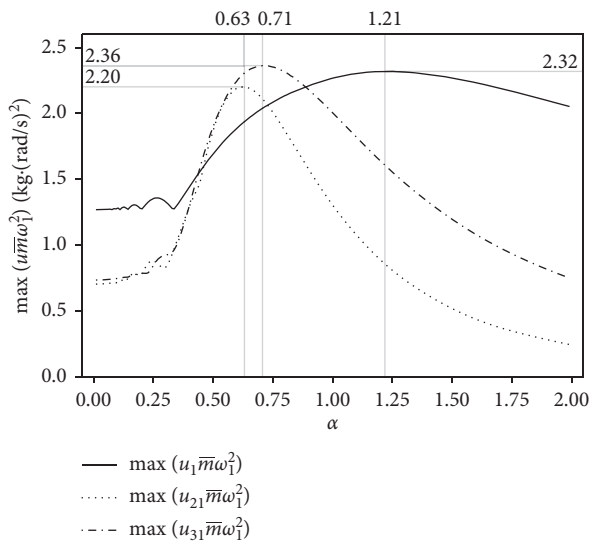

Figure 6: The maximum displacement curves of the beam under three kinds of moving load conditions with different speed parameter α ($n = 1$; $\eta = 1.3$; $\beta_m = 0$; α is from 0 to 2).

4. Multispan Continuous Beam

For a multispan continuous beam as shown in Figure 7, the local coordinate x_i $(i = 1, 2, \ldots, N)$ for each span is introduced, while x stands for the global coordinate for the whole beam. N is the number of spans. The mode shape of the multispan continuous beam can be written as $\phi_m(\xi_m, x)$ for the global coordinate x and $\phi_{mi}(\xi_m, x_i)$ for each span in the local coordinate x_i.

Based on the modal superposition method, the general equation of the continuous beam can be solved as

$$\frac{d^2 q_m(t)}{dt^2} + 2\zeta_m \omega_m \frac{dq_m(t)}{dt} + \omega_m^2 q_m(t) = \frac{1}{\overline{m}\widetilde{\phi}_m} \sum_{i=1}^{N} \int_0^{L_i} f(x_i, t)\phi_{mi} \mathrm{d}x_i, \tag{18}$$

where L_i is the length of the ith span of continuous beam, q_m is the mth modal coordinate of continuous beam, and

$$\widetilde{\phi}_m = \int_0^L \phi_m^2(\xi_m, x)\mathrm{d}x = \sum_{i=1}^{N} \int_0^{L_i} \phi_{mi}^2(\xi_m, x_i)\mathrm{d}x_i. \tag{19}$$

Equation (18) can be deemed as the summation of the responses of the system acted by $\int_0^{L_i} f(x_i, t)\phi_{mi}/(\overline{m}\widetilde{\phi}_m)\mathrm{d}x_i$, which can be considered as the distributed force just acting upon the ith span of the beam. The response equation can be written as

$$\frac{d^2 q_{mi}(t)}{dt^2} + 2\zeta_m \omega_m \frac{dq_{mi}(t)}{dt} + \omega_m^2 q_{mi}(t) = \frac{1}{\overline{m}\widetilde{\phi}_m} \int_0^{L_i} f(x_i, t)\phi_{mi} \mathrm{d}x_i, \tag{20}$$

where q_{mi} stands for the solution of the modal coordinate of continuous beam when the distributed force is just acting on the ith span of the beam. This equation can be solved by the general model in Section 2. Then, q_m can be solved by

$$q_m(t) = \sum_{i=1}^{N} q_{mi}(t). \tag{21}$$

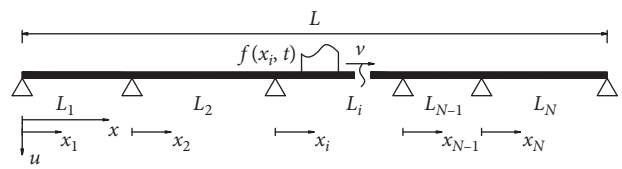

Figure 7: N-span continuous beam.

5. Distributed Form of Dynamic Pressure due to the Train Gust

Figure 8 shows a pressure signal produced by a high-speed train at a point under a platform canopy, which is located on the Beijing-Shanghai high-speed railway in China. When the train arrives, the air pressure experiences a positive peak followed by a negative (suction) peak due to the head of train passing. When the train leaves, the air pressure experiences a suction peak followed by a positive peak due to the tail of train passing [38]. And as the coupler of train passing, the air pressure experiences a suction peak followed by a positive peak, then drops to a suction peak again. From the spatial perspective, each point along the trackside experiences the dynamic pressures due to train gust, which are related with the distance between the point and the train, the speed, and the shape of the train. For flat horizontal or vertical structures parallel to the tracks, the aerodynamic loads can be deemed as distributed forces moving at the speed of train that has been proved by the site test and computational fluid dynamics (CFD) calculations and suggested by some railway standards [39, 40]. Thus, the air pressure in Figure 8 is considered to be caused by three segments of distributed forces, which are corresponding to the moving of head, coupler, and tail, respectively. The relationship between the distributed force and the pressure signal will be studied in the following section.

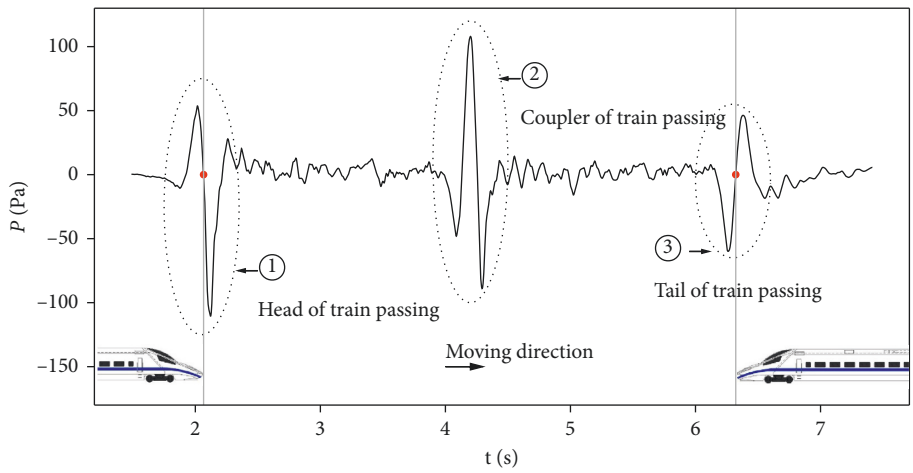

Figure 8: Air pressure signal produced by a high-speed train at a point under a platform canopy.

5.1. Relationship between the Distributed Force and the Pressure Signal of a Point. A distributed force moving at a constant speed of v is illustrated in Figure 9. When the distributed force passes by a point, the pressure signal of the point due to the distributed force can be expressed as $f(t)$ as shown in Figure 9(a). Suppose the point is located at 0 in the global coordinate x, the pressure at t_1 is equal to $f(\tilde{x}_1)$, where

$$\tilde{x}_1 = \tilde{L} - vt_1. \tag{22}$$

According to equation (1), there are three steps of changing from $f(\tilde{x})$ to $f(t)$, as shown in Figure 9(b). In practice, the pressure signal is more accessible than the distributed force. Therefore, the distributed force can be obtained from pressure signal of a point by equation (22) and reversing the procedure of Figure 9(b).

5.2. Fourier Series Representation of Distributed Force Solved by Using FFT. For most engineering practice, the pressure signal is sampled with a discrete set of equally spaced points $f(k\Delta t)$, $k = 0, 1, 2, \ldots, M-1$ [41]. M is the number of sampled points. According to Section 5.1, the distributed force can be solved with the same volume of discrete set of equally spaced points $f(k\Delta x)$, $\Delta x = \tilde{L}/M$. The relationship between Fourier series coefficients and discrete samples has been studied by Tomas [42]. More details of the Fourier series representation of distributed force solved by using FFT are listed by authors. The discrete Fourier transform g_n $(n = 0, 1, 2, \ldots, M-1)$ of a set of points $f(k\Delta x)$, $k = 0, 1, 2, \ldots, M-1$ can be defined as

$$g_n = \sum_{k=0}^{M-1} f(k\Delta x)\exp\left(-i\frac{2\pi nk}{M}\right). \tag{23}$$

According to Euler's identity, equation (23) can be reexpressed as

$$g_n = g_{cn} - ig_{sn}, \tag{24}$$

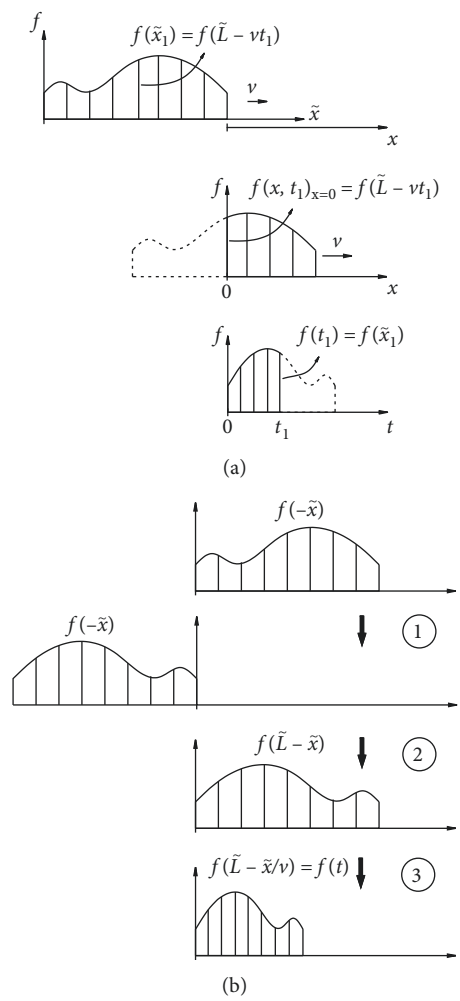

Figure 9: A distributed force moving at a constant speed of v. (a) Relationship between the pressure signal of a point and the distributed force. (b) Procedure of changing from $f(\tilde{x})$ to $f(t)$.

where g_{cn} and g_{sn} are the Fourier cosine and sine transform of signal f, which can be calculated by fast Fourier transformation (FFT) and expressed as

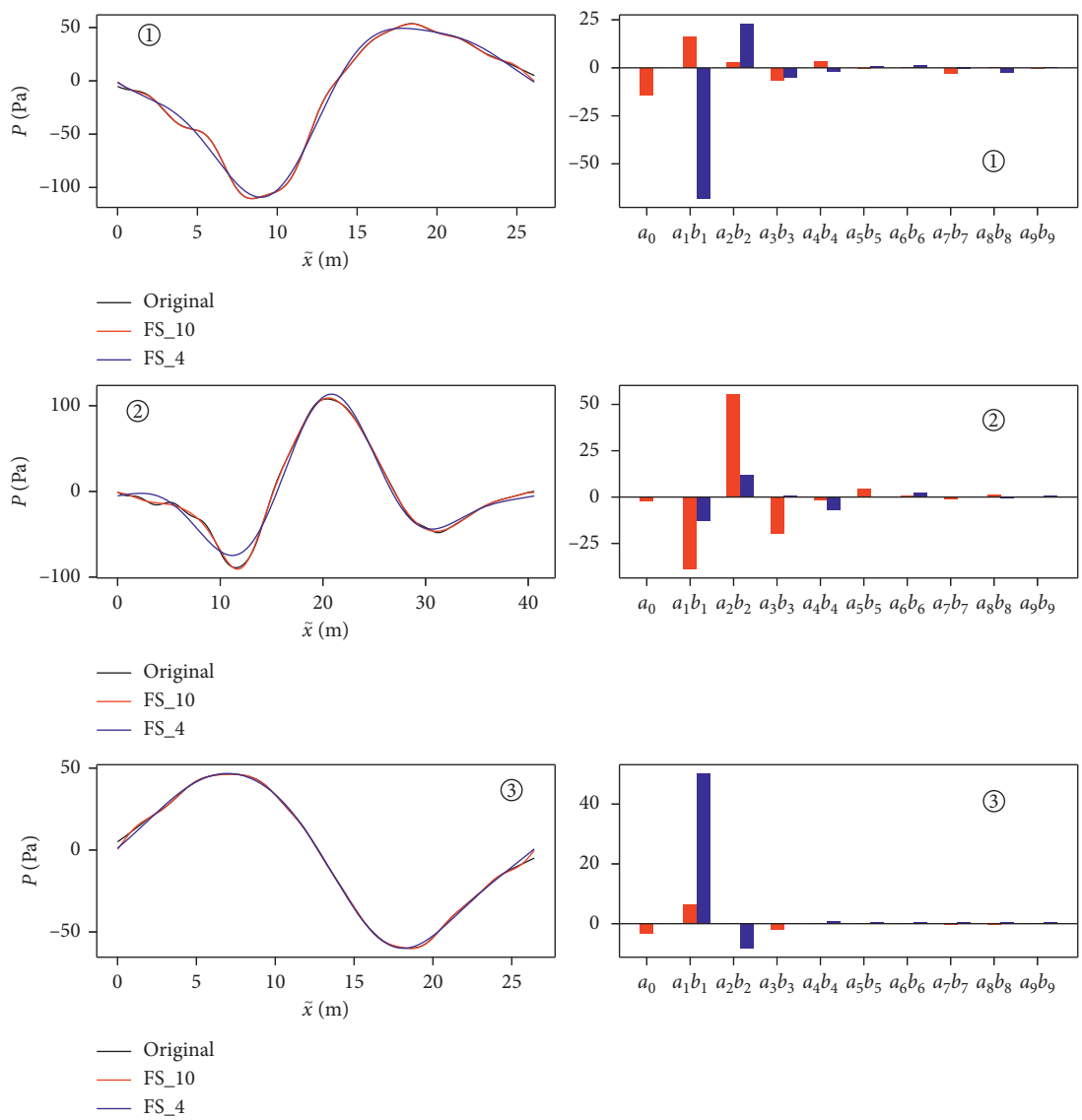

Figure 10: Distributed forces transformed from the pressure signal in Figure 8 and its Fourier series representations (FS_10 and FS_4 represent first-10 and first-4 Fourier series representations, respectively).

$$g_{cn} = \mathrm{Re}(g_n) = \sum_{k=0}^{M-1} f(k\Delta x)\cos\left(\frac{2\pi nk}{M}\right),$$
$$g_{sn} = -\mathrm{Im}(g_n) = \sum_{k=0}^{M-1} f(k\Delta x)\sin\left(\frac{2\pi nk}{M}\right). \tag{25}$$

Using the trapezoidal rule, the integral of the Fourier series coefficients a_0, a_n, and b_n in equations (8a), (8b), and (8c) can be approximated by

$$a_0 \approx \frac{1}{M}\sum_{k=0}^{M-1} f(k\Delta x) = \frac{g_{c0}}{M}, \tag{26a}$$

$$a_n \approx \frac{2}{M}\sum_{k=0}^{M-1} f(k\Delta x)\cos\left(\frac{2\pi nk}{M}\right) = \frac{2g_{cn}}{M}, \tag{26b}$$

$$b_n \approx \frac{2}{M}\sum_{k=0}^{M-1} f(k\Delta x)\sin\left(\frac{2\pi nk}{M}\right) = \frac{2g_{sn}}{M}. \tag{26c}$$

According to the abovementioned methods, the three segments of distributed forces can be transformed from the air pressure signal in Figure 8, corresponding to the passing by the head, coupler, and tail of the train, respectively, as shown in Figure 10. Meanwhile, the Fourier series coefficients and Fourier series representations are given. For the first and the third segment of distributed force, the contribution of the first sine wave to the distributed forces due to the head and tail of train is the biggest. But for the second segment of distributed force due to the coupler, the first and second cosine waves account for a large proportion. It can be seen that the first 4 Fourier series representations achieve good approximations of the three segments of

Table 1: Parameters of the purlin.

E (GPa)	I (m^4)	$\overline{m}$ (kg/m)	L_1 (m)	$\xi_1 L_1$	v_{cr} (m/s)	ζ_m
206	4.29×10^{-4}	106.42	24	π	119.29	0.03

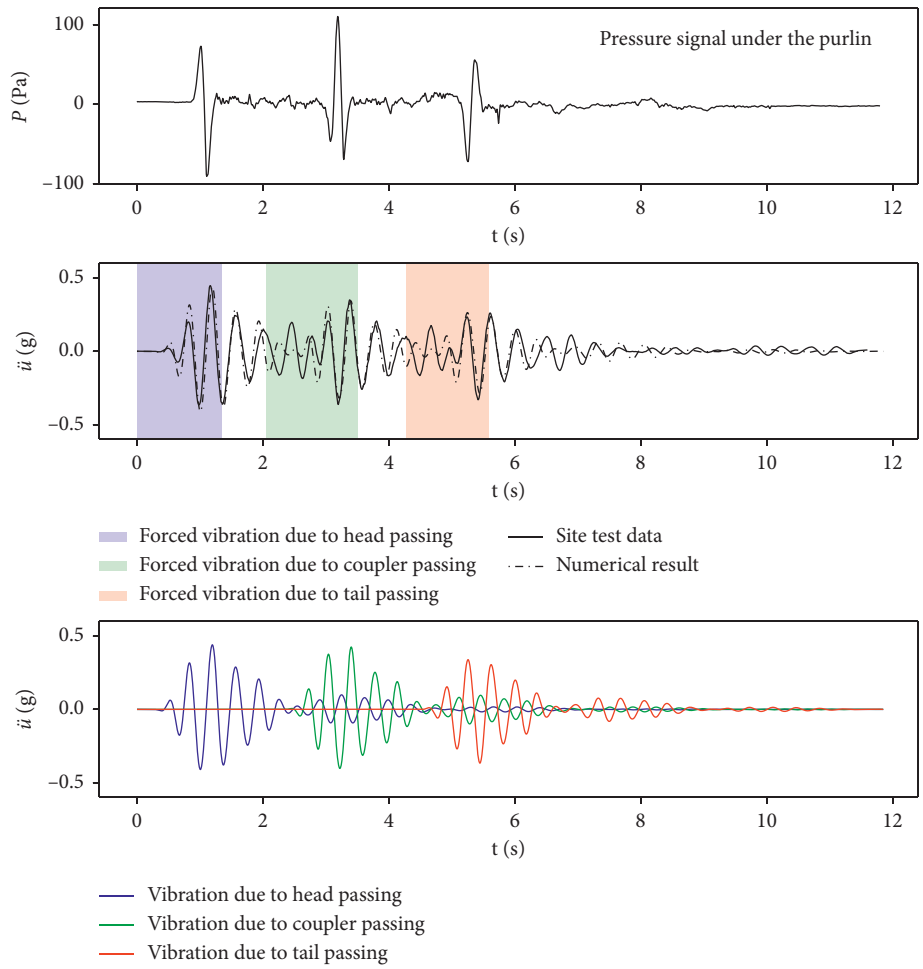

Figure 11: Pressure signal and comparison of accelerations of the purlin between site test data and numerical result for the high-speed train with speed 344.797 km/h.

distributed force, and the first 10 Fourier series representations can achieve excellent approximations.

6. Numerical Results

To further explore the relationship between dynamic pressure and vibrations of the structure, a site test was conducted on the platform canopy discussed in Section 5. The canopy is a steel structure, whose roof system consists of continuous H-section purlins, insulating layer, decorative layer, and metal roof panels. Each purlin is parallel to the tracks, with 4 spans of 24 m each and regular intervals of 2.5 m. Three piezoresistive pressure transducers were located under a purlin and near the decorative layer for sampling the dynamic pressure acting upon the purlin. A capacitive acceleration sensor was located on the center of the fourth span of the purlin to validate the dynamic response. From structural aspect, the purlin can be deemed as a 4-span continuous beam, whose parameters are illustrated in Table 1. It should be noted that all the parameters are calculated from the construction drawing of the platform canopy except the damping factors ζ_m, which are assumed to be 0.03 for steel structures generally.

Measurements were made on two high-speed trains, which passed the canopy with different speeds: 95.777 m/s (344.797 km/h) and 86.715 m/s (312.174 km/h). The pressure signals under the purlin are illustrated in Figures 11 and 12, respectively. The speed parameter α can be calculated with the results: 0.803 and 0.727. The comparisons of acceleration of the purlin between site test data and numerical result are also illustrated in Figures 11 and 12. It is shown that there is a good consistency between the numerical result and site test data in the forced vibration phase and some difference in the free-vibration phase. The main reason of the difference is the

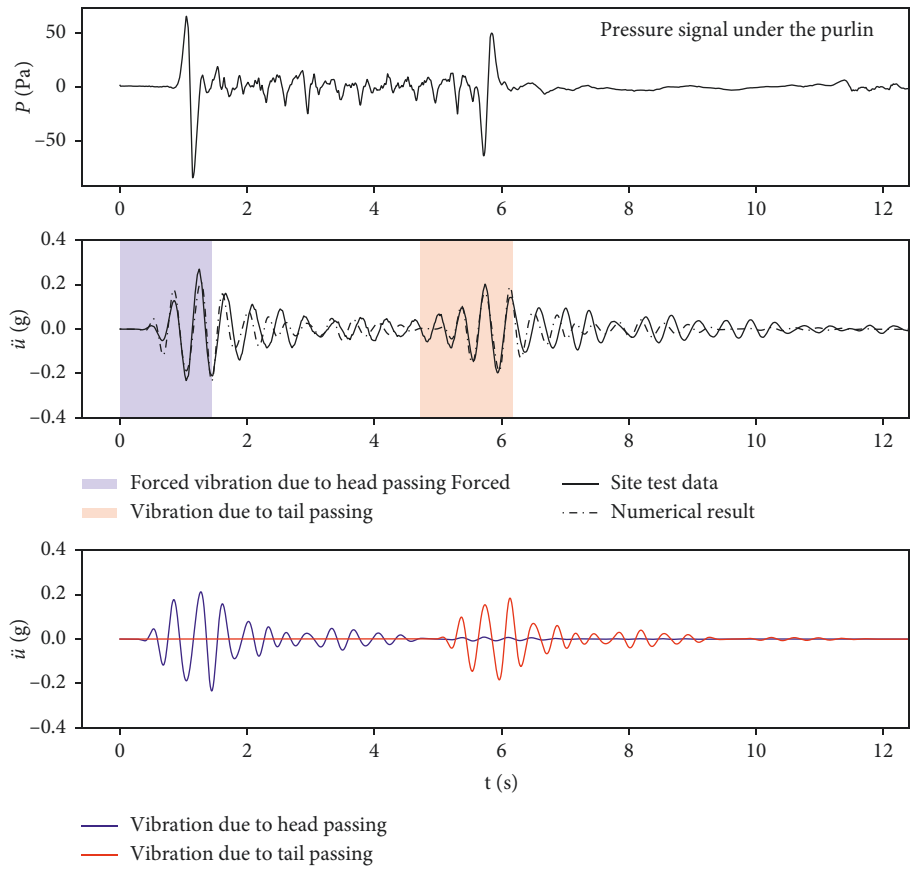

Figure 12: Pressure signal and comparison of accelerations of the purlin between site test data and numerical result for the high-speed train with speed 312.174 km/h.

damping factors ζ_m of the real structure are not equal to the assumed value 0.03. If the actual structural parameters are given, there will be better numerical results. We will not discuss this since the actual structural parameters need to be identified by other methods, which are out of scope of this paper. From the aspect of dynamic response analysis, more concerns are about the maximum displacement, velocity, and acceleration as well. From the two figures, the maximum acceleration is not remarkably affected by the assumed damping factor. Thus, the numerical results are credible. The response of the continuous beam can be decomposed into different parts due to the passing of head, coupler, and tail, respectively, as shown in the third subfigures of the two figures. There are cancellation phenomena between the three parts of vibrations, which are related with the speed of train, the parameters of structure, and the distance between the head, coupler, and tail. Obviously, the cancellation phenomenon will be changed to resonance phenomenon under some conditions. Thus, this should be considered in engineering practice, especially for light damping structures along the track sides.

In dynamics, the ratio of vibration amplitude to the static displacement which would be produced by the same load can be used to estimate the dynamic amplification effect. For this problem, the central displacements of each span of the 4-span continuous purlin due to the two high-speed trains passing are illustrated in Figures 13 and 14. It should be noted that the static displacement of the continuous beam can be calculated by the same procedure for solving the dynamic displacement and just neglecting the inertia force and the damping force. Since the 4-span continuous purlin is symmetrical about the middle support, there is a symmetric phenomenon of the static displacement between the first two spans and the the last two spans. The maximum dynamic displacements happen at the fourth span of the purlin, with maximum values 16.8 mm and 9.5 mm due to the head of the two high-speed trains passing, which are about 4.4 and 3.0 times as much as the maximum static displacements under the same conditions.

Figure 15 shows the comparisons of the distributed force due to the head passing, Fourier series coefficients, and central displacements of the fourth span of the purlin between the two high-speed trains. The maximum positive and negative pressures are 66.1 Pa and 83.3 Pa, 73.3 Pa and 90.4 Pa for the head of the two trains passing, respectively. The absolute value of the first sine coefficient increases about

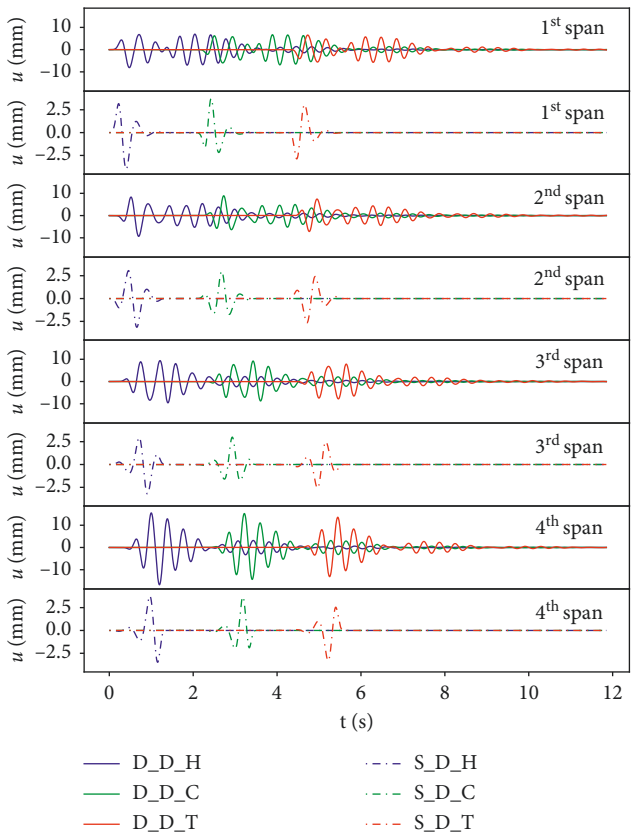

Figure 13: Central displacements of each span of the 4-span continuous purlin due to the high-speed train passing with speed 344.797 km/h (S_D_H, S_D_C, and S_D_T stand for static displacements of the purlin due to the passing of head, coupler, and tail, respectively; D_D_H, D_D_C, and D_D_T stand for dynamic displacements of the purlin due to the passing of head, coupler, and tail, respectively).

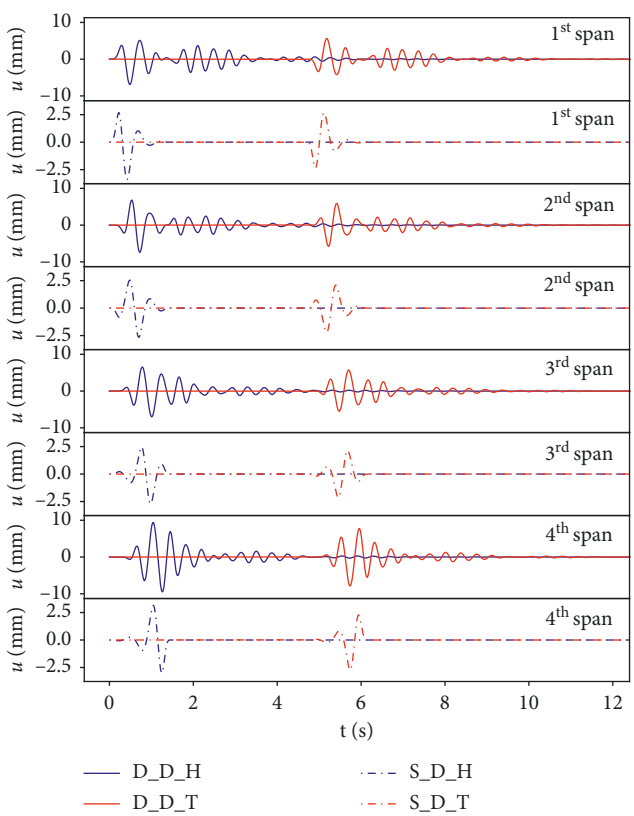

Figure 14: Central displacements of each span of the 4-span continuous purlin due to the high-speed train passing with speed 312.174 km/h (S_D_H and S_D_T stand for static displacements of the purlin due to the passing of head and tail, respectively; D_D_H and D_D_T stand for dynamic displacements of the purlin due to the passing of head and tail, respectively).

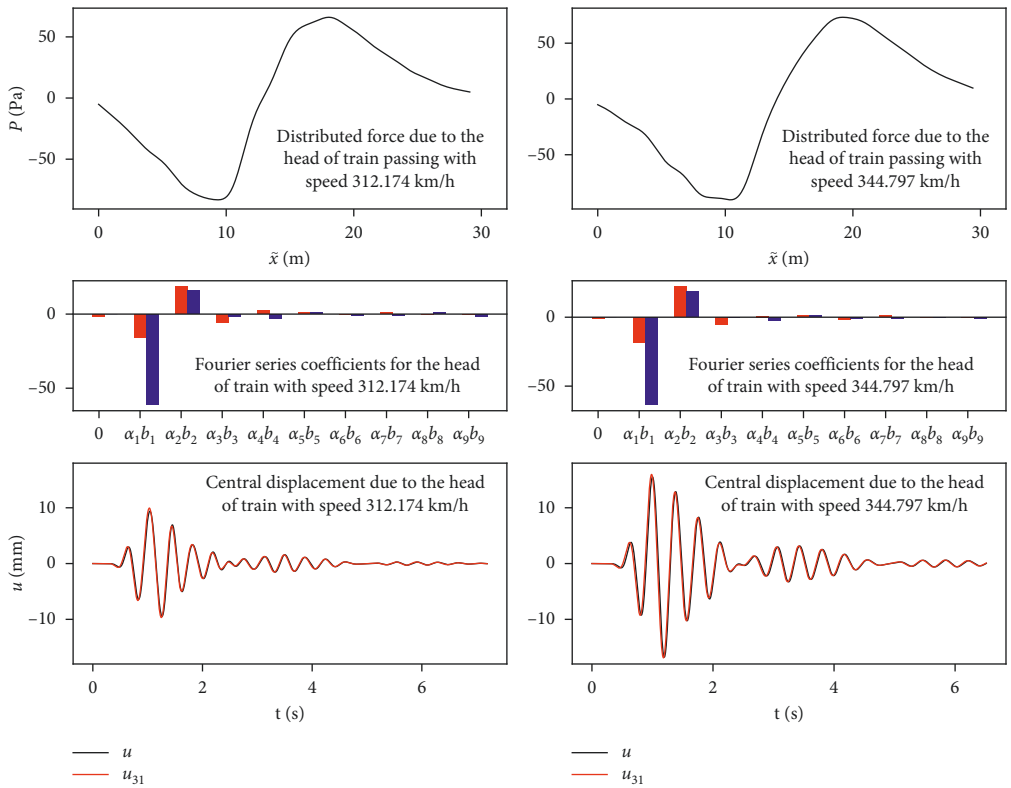

Figure 15: Comparisons of the distributed force, Fourier series coefficients, and central displacements of the fourth span of the purlin between the two high-speed trains (u stands for the central displacement of the purlin under the distributed force due to the head of the train and u_{31} stands for the central displacement of the purlin under the first sine wave decomposed from the distributed force due to the head of the train).

3.92% (from 61.2 to 63.6) when the speed of the train increases about 10.5% (from 86.715 m/s to 95.777 m/s). Under these two moving distributed forces, the maximum value of central displacement of the purlin increases about 76.8% (from 9.5 mm to 16.8 mm). We should pay more attention to this dynamic amplification effect in the structures along the tracksides when the trains run at high speed. The central displacements of purlin u_{31} under the first sine waves due to the head of the trains are also illustrated in Figure 15. The results of u_{31} are similar to the results of u, and the first sine wave can be used to evaluate the dynamic response of the beam due to the train gust for simplifying the calculation.

7. Conclusions

This study developed a general method to solve the dynamic response of an Euler–Bernoulli beam subjected to moving distributed force. The response of a single-span beam with general boundary conditions under moving distributed force was studied first. Then, the theory was extended to multispan continuous beam. By decomposing the distributed force into Fourier series representations, the total response of a beam under moving distributed force was written as the summation of the responses of the beam under each item of Fourier series representations. Then, the individual results were solved by using the mode superposition method and Duhamel integral formulation. The comparisons of dynamic results demonstrate that the proposed method has higher accuracy and computational efficiency than FEM. Considering the pressure signal of a point is more accessible than the distributed force in practice, and a method was suggested to get the distributed force from a pressure signal of a point. The Fourier series representations of distributed force can be solved by using FFT. The following can be concluded from the numerical results:

(1) The contribution of the first sine wave due to the head and tail of the train passing is the biggest among all the Fourier series. The response of the beam under the first sine wave has a good approximation to the total response of the beam when the head and tail of the train is passing.

(2) Resonance phenomenon should be considered in engineering practice, especially for light damping structures along the tracksides.

(3) The dynamic amplification effect on the structures along the tracksides deserves much attention when the trains run at high speed.

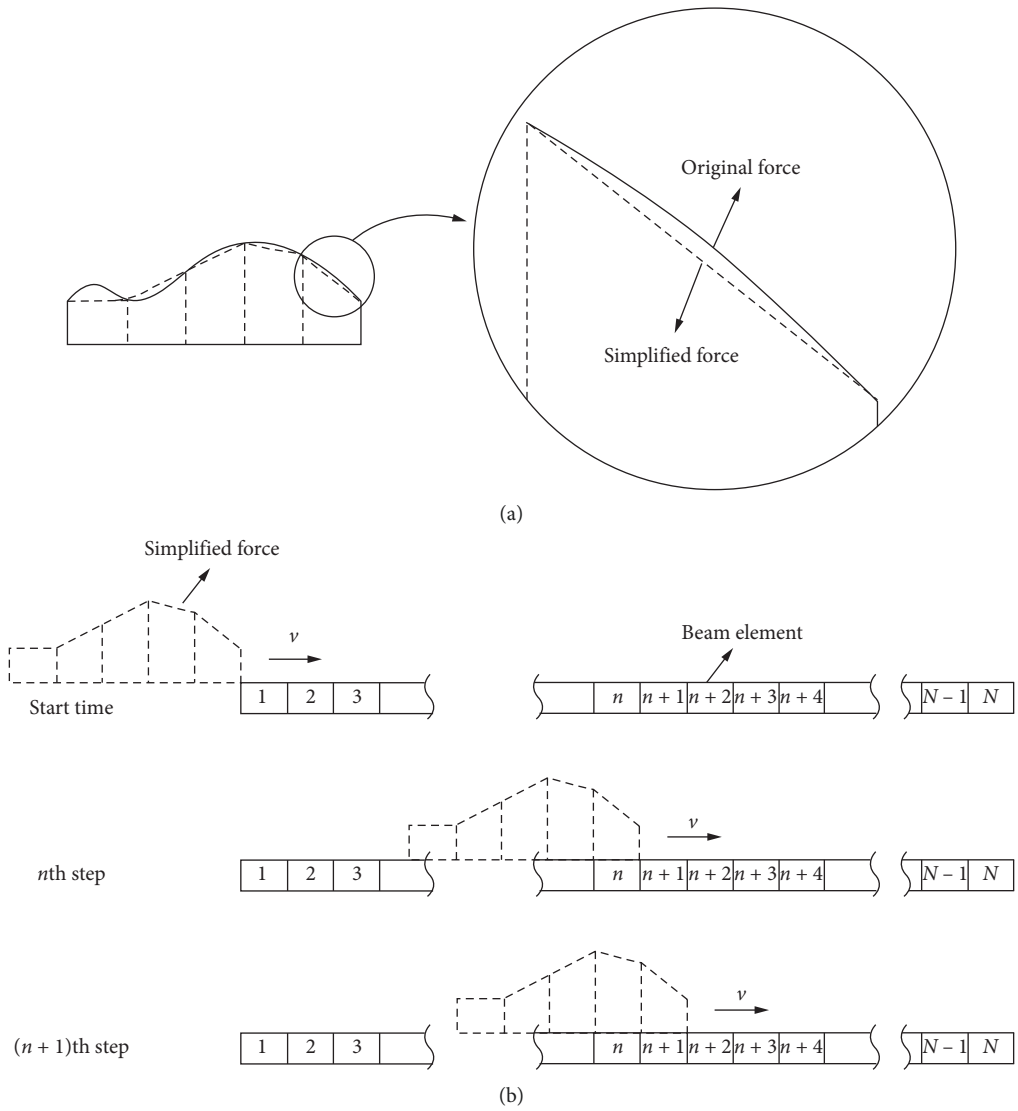

Figure 16: Finite element procedure for solving moving distributed force problem. (a) Original distributed force and the simplified force. (b) Simplified force at each time step.

Abbreviations

α:	Dimensionless speed parameter
β_m:	Dimensionless damping parameter
η:	Length ratio of the distributed force to the beam, $\eta = \widetilde{L}/L$
$\widehat{\phi}_m$:	$\widehat{\phi}_m = \widetilde{\phi}_m/L$
λ_m:	Ratio of the mth eigenvalue to the first, $\lambda_m = \xi_m/\xi_1$
$\mathbf{A}_m$:	$\mathbf{A}_m = \left[A_m \;\; B_m \;\; C_m \;\; D_m \right]^T$
ω_D^m:	Damped vibration frequency corresponding to the mth mode, $\omega_D^m = \omega_m \sqrt{1 - \zeta_m^2}$
ω_m:	mth circular frequency of beam, $\omega_m = \xi_m^2 \sqrt{EI/\overline{m}}$
$\overline{m}$:	Mass per unit length of beam
$\phi_m(\xi_m, x)$:	mth mode shape of beam
$\widetilde{\phi}_m$:	$\widetilde{\phi}_m = \int_0^L \phi_m^2(\xi_m, x)\mathrm{d}x$
$\widetilde{f}_1$, $\widetilde{f}_{2n}$, and $\widetilde{f}_{3n}$:	Distributed forces in the base models
$\widetilde{L}$:	Length of the distributed force
$\widetilde{q}_{1m}$, $\widetilde{q}_{2nm}$, and $\widetilde{q}_{3nm}$:	mth modal coordinates of the base models
$\widetilde{u}_1$, $\widetilde{u}_{2n}$, and $\widetilde{u}_{3n}$:	Transverse deflections of beam under $\widetilde{f}_1$, $\widetilde{f}_{2n}$, and $\widetilde{f}_{3n}$
$\widetilde{x}$:	Local coordinate for the distributed force
ξ_m:	mth eigenvalue of beam
ζ_m:	mth damping ratio of beam, $\zeta_m = c/(2\overline{m}\omega_m)$
a_0, a_n, and b_n:	Fourier series coefficients
A_m, B_m, C_m, and D_m:	Coefficients of the mth mode shape
c:	Structural damping of beam
E:	Young's modulus of material
f_1, f_{2n}, and f_{3n}:	Fourier series representations of the distributed force

g_n:	Fourier transform
g_{cn} and g_{sn}:	Fourier cosine and sine transform
$H(\tilde{x})$:	Heaviside unit function
I:	Moment of inertia of beam-section
L:	Length of the beam
L_i:	Length of the ith span of continuous beam
M:	Number of sampled points
N:	Span number of continuous beam
$q_m(t)$:	mth modal coordinate of continuous beam
q_{mi}:	Solution of modal coordinate of the continuous beam when the distributed force is just acting on the ith span of the beam
t:	Time
u:	Transverse deflection of beam
v:	Speed of the distributed force
x:	Global coordinate for the whole system
$\tilde{x}$:	Local coordinate for the distributed force.

Appendix

A. Details of Modal Forces p_{2nm} and p_{3nm}

$$p_{2nm}(t) = \frac{a_n}{\overline{m}\tilde{\phi}_m}\int_0^L \cos\left[\frac{2\pi n(x-vt)}{\tilde{L}}\right][1-H(x-vt)]\phi_m(\xi_m,x)dx = \begin{cases} \dfrac{a_n}{\overline{m}\tilde{\phi}_m\xi_m}\Gamma_{2nm}(t)\mathbf{A}_m, & 0\le t\le t_1, \\ \dfrac{a_n}{\overline{m}\tilde{\phi}_m\xi_m}\Pi_{2nm}(t)\mathbf{A}_m, & t>t_1, \end{cases} \tag{A.1}$$

$$p_{3nm}(t) = \frac{b_n}{\overline{m}\tilde{\phi}_m}\int_0^L \sin\left[\frac{2\pi n(x-vt)}{\tilde{L}}\right][1-H(x-vt)]\phi_m \cdot (\xi_m,x)\mathrm{d}x = \begin{cases} \dfrac{b_n}{\overline{m}\tilde{\phi}_m\xi_m}\Gamma_{3nm}(t)\mathbf{A}_m, & 0\le t\le t_1, \\ \dfrac{b_n}{\overline{m}\tilde{\phi}_m\xi_m}\Pi_{3nm}(t)\mathbf{A}_m, & t>t_1, \end{cases} \tag{A.2}$$

where

$$t_1 = \frac{\xi_1 L}{\omega_1\alpha},$$

$$\Gamma_{2nm}(t) = [\,\gamma_{2nm1}\ \ \gamma_{2nm2}\ \ \gamma_{2nm3}\ \ \gamma_{2nm4}\,],$$

$$\Pi_{2nm}(t) = [\,\gamma_{2nm5}\ \ \gamma_{2nm6}\ \ \gamma_{2nm7}\ \ \gamma_{2nm8}\,],$$

$$\Gamma_{3nm}(t) = [\,\gamma_{3nm1}\ \ \gamma_{3nm2}\ \ \gamma_{3nm3}\ \ \gamma_{3nm4}\,],$$

$$\Pi_{3nm}(t) = [\,\gamma_{3nm5}\ \ \gamma_{3nm6}\ \ \gamma_{3nm7}\ \ \gamma_{3nm8}\,],$$

in which

$$\gamma_{2nm1} = \frac{\lambda_m\gamma^t_{\omega,7} - \lambda_m\gamma^t_{\omega,3}}{(\lambda_m^2 - Q_n^2)\xi_1}, \tag{A.3}$$

$$\gamma_{2nm2} = \frac{-Q_n\gamma^t_{\omega,8} + \lambda_m\gamma^t_{\omega,4}}{(\lambda_m^2 - Q_n^2)\xi_1}, \tag{A.4}$$

$$\gamma_{2nm3} = \frac{-\lambda_m\gamma^t_{\omega,7} + \lambda_m\gamma^t_{\omega,5}}{(\lambda_m^2 + Q_n^2)\xi_1}, \tag{A.5}$$

$$\gamma_{2nm4} = \frac{Q_n\gamma^t_{\omega,8} + \lambda_m\gamma^t_{\omega,6}}{(\lambda_m^2 + Q_n^2)\xi_1}, \tag{A.6}$$

$$\gamma_{2nm5} = \frac{\psi_1\gamma^t_{\omega,8} + \psi_2\gamma^t_{\omega,7}}{(\lambda_m^2 - Q_n^2)\xi_1}, \tag{A.7}$$

$$\gamma_{2nm6} = \frac{\psi_3\gamma^t_{\omega,8} - \psi_4\gamma^t_{\omega,7}}{(\lambda_m^2 - Q_n^2)\xi_1}, \tag{A.8}$$

$$\gamma_{2nm7} = \frac{\psi_5\gamma^t_{\omega,8} - \psi_6\gamma^t_{\omega,7}}{(\lambda_m^2 + Q_n^2)\xi_1}, \tag{A.9}$$

$$\gamma_{2nm8} = \frac{\psi_7\gamma^t_{\omega,8} + \psi_8\gamma^t_{\omega,7}}{(\lambda_m^2 + Q_n^2)\xi_1}, \tag{A.10}$$

$$\gamma_{3nm1} = \frac{-\lambda_m\gamma^t_{\omega,8} + Q_n\gamma^t_{\omega,4}}{(\lambda_m^2 - Q_n^2)\xi_1}, \tag{A.11}$$

$$\gamma_{3nm2} = \frac{-Q_n\gamma^t_{\omega,7} + Q_n\gamma^t_{\omega,3}}{(\lambda_m^2 - Q_n^2)\xi_1}, \tag{A.12}$$

$$\gamma_{3nm3} = \frac{\lambda_m\gamma^t_{\omega,8} - Q_n\gamma^t_{\omega,6}}{(\lambda_m^2 + Q_n^2)\xi_1}, \tag{A.13}$$

$$\gamma_{3nm4} = \frac{Q_n\gamma^t_{\omega,7} - Q_n\gamma^t_{\omega,5}}{(\lambda_m^2 + Q_n^2)\xi_1}, \tag{A.14}$$

$$\gamma_{3nm5} = \frac{\psi_1\gamma^t_{\omega,7} - \psi_2\gamma^t_{\omega,8}}{(\lambda_m^2 - Q_n^2)\xi_1}, \tag{A.15}$$

$$\gamma_{3nm6} = \frac{\psi_3\gamma^t_{\omega,7} + \psi_4\gamma^t_{\omega,8}}{(\lambda_m^2 - Q_n^2)\xi_1}, \tag{A.16}$$

$$\gamma_{3nm7} = \frac{\psi_5\gamma^t_{\omega,7} + \psi_6\gamma^t_{\omega,8}}{(\lambda_m^2 + Q_n^2)\xi_1}, \tag{A.17}$$

$$\gamma_{3nm8} = \frac{\psi_7\gamma^t_{\omega,7} - \psi_8\gamma^t_{\omega,8}}{(\lambda_m^2 + Q_n^2)\xi_1}, \tag{A.18}$$

$$
\begin{aligned}
Q_n &= \frac{2n\pi}{\eta\xi_1 L},\\
\psi_1 &= Q_n \sin(\lambda_m\xi_1 L)\cos(Q_n\xi_1 L)\\
&\quad - \lambda_m \cos(\lambda_m\xi_1 L)\sin(Q_n\xi_1 L),\\
\psi_2 &= \lambda_m - \lambda_m \cos(\lambda_m\xi_1 L)\cos(Q_n\xi_1 L)\\
&\quad - Q_n \sin(\lambda_m\xi_1 L)\sin(Q_n\xi_1 L),\\
\psi_3 &= -Q_n + Q_n \cos(\lambda_m\xi_1 L)\cos(Q_n\xi_1 L)\\
&\quad + \lambda_m \sin(\lambda_m\xi_1 L)\sin(Q_n\xi_1 L),\\
\psi_4 &= Q_n \cos(\lambda_m\xi_1 L)\sin(Q_n\xi_1 L)\\
&\quad - \lambda_m \sin(\lambda_m\xi_1 L)\cos(Q_n\xi_1 L),\\
\psi_5 &= \lambda_m\cosh(\lambda_m\xi_1 L)\sin(Q_n\xi_1 L)\\
&\quad - Q_n\sinh(\lambda_m\xi_1 L)\cos(Q_n\xi_1 L),\\
\psi_6 &= \lambda_m - \lambda_m\cosh(\lambda_m\xi_1 L)\cos(Q_n\xi_1 L)\\
&\quad - Q_n\sinh(\lambda_m\xi_1 L)\sin(Q_n\xi_1 L),\\
\psi_7 &= Q_n - Q_n\cosh(\lambda_m\xi_1 L)\cos(Q_n\xi_1 L)\\
&\quad + \lambda_m\sinh(\lambda_m\xi_1 L)\sin(Q_n\xi_1 L),\\
\psi_8 &= Q_n\cosh(\lambda_m\xi_1 L)\sin(Q_n\xi_1 L)\\
&\quad + \lambda_m\sinh(\lambda_m\xi_1 L)\cos(Q_n\xi_1 L),\\
\gamma_{\omega,3}^{t} &= \cos(\alpha\lambda_m\omega_1 t),\\
\gamma_{\omega,4}^{t} &= \sin(\alpha\lambda_m\omega_1 t),\\
\gamma_{\omega,5}^{t} &= \cosh(\alpha\lambda_m\omega_1 t),\\
\gamma_{\omega,6}^{t} &= \sinh(\alpha\lambda_m\omega_1 t),\\
\gamma_{\omega,7}^{t} &= \cos(\alpha Q_n\omega_1 t),\\
\gamma_{\omega,8}^{t} &= \sin(\alpha Q_n\omega_1 t).
\end{aligned}
\tag{A.19}
$$

B. Parameters of $\widehat{\Gamma}_{1m}$ and $\breve{\Gamma}_{1m}$

$$\widehat{\Gamma}_{1m} = [\,\widehat{\gamma}_{11}\ \ \widehat{\gamma}_{12}\ \ \widehat{\gamma}_{13}\ \ \widehat{\gamma}_{14}\,], \tag{B.1}$$

$$\breve{\Gamma}_{1m} = [\,\breve{\gamma}_{11}\ \ \breve{\gamma}_{12}\ \ \breve{\gamma}_{13}\ \ \breve{\gamma}_{14}\,], \tag{B.2}$$

$$\widehat{\gamma}_{11} = \gamma\gamma_{11}(t) - \gamma\gamma_{15}(t), \tag{B.3}$$

$$\widehat{\gamma}_{12} = \gamma\gamma_{12}(t) + \gamma\gamma_{16}(t), \tag{B.4}$$

$$\widehat{\gamma}_{13} = \gamma\gamma_{13}(t) + \gamma\gamma_{17}(t), \tag{B.5}$$

$$\widehat{\gamma}_{14} = \gamma\gamma_{14}(t) + \gamma\gamma_{18}(t), \tag{B.6}$$

$$
\begin{aligned}
\breve{\gamma}_{11} &= \gamma\gamma_{11}(t) - \gamma\gamma_{11}(t-t_1)\cos(\lambda_m\xi_1 L)\\
&\quad - \gamma\gamma_{12}(t-t_1)\sin(\lambda_m\xi_1 L),
\end{aligned}
\tag{B.7}
$$

$$
\begin{aligned}
\breve{\gamma}_{12} &= \gamma\gamma_{12}(t) - \gamma\gamma_{12}(t-t_1)\cos(\lambda_m\xi_1 L)\\
&\quad + \gamma\gamma_{11}(t-t_1)\sin(\lambda_m\xi_1 L),
\end{aligned}
\tag{B.8}
$$

$$
\begin{aligned}
\breve{\gamma}_{13} &= \gamma\gamma_{13}(t) - \gamma\gamma_{13}(t-t_1)\cosh(\lambda_m\xi_1 L)\\
&\quad - \gamma\gamma_{14}(t-t_1)\sinh(\lambda_m\xi_1 L),
\end{aligned}
\tag{B.9}
$$

$$
\begin{aligned}
\breve{\gamma}_{14} &= \gamma\gamma_{14}(t) - \gamma\gamma_{14}(t-t_1)\cosh(\lambda_m\xi_1 L)\\
&\quad - \gamma\gamma_{13}(t-t_1)\sinh(\lambda_m\xi_1 L),
\end{aligned}
\tag{B.10}
$$

where

$$
\begin{aligned}
\gamma\gamma_{11}(t) &= \gamma\gamma_{1,0}^{\lambda_m} + \gamma\gamma_{1,1}^{\lambda_m,\alpha,\beta_m}\gamma_{\omega,1}^{t} + \gamma\gamma_{1,3}^{\lambda_m,\alpha,\beta_m}\gamma_{\omega,2}^{t},\\
\gamma\gamma_{12}(t) &= \gamma\gamma_{1,5}^{\lambda_m,\alpha,\beta_m}\gamma_{\omega,1}^{t} - \gamma\gamma_{1,9}^{\lambda_m,\alpha,\beta_m}\gamma_{\omega,2}^{t},\\
\gamma\gamma_{13}(t) &= -\gamma\gamma_{1,0}^{\lambda_m} + \gamma\gamma_{1,2}^{\lambda_m,\alpha,\beta_m}\gamma_{\omega,1}^{t} + \gamma\gamma_{1,4}^{\lambda_m,\alpha,\beta_m}\gamma_{\omega,2}^{t},\\
\gamma\gamma_{14}(t) &= \gamma\gamma_{1,6}^{\lambda_m,\alpha,\beta_m}\gamma_{\omega,1}^{t} - \gamma\gamma_{1,10}^{\lambda_m,\alpha,\beta_m}\gamma_{\omega,2}^{t},\\
\gamma\gamma_{15}(t) &= \gamma\gamma_{1,7}^{\lambda_m,\alpha,\beta_m}\gamma_{\omega,3}^{t} + \gamma\gamma_{1,5}^{\lambda_m,\alpha,\beta_m}\gamma_{\omega,4}^{t},\\
\gamma\gamma_{16}(t) &= \gamma\gamma_{1,7}^{\lambda_m,\alpha,\beta_m}\gamma_{\omega,4}^{t} - \gamma\gamma_{1,5}^{\lambda_m,\alpha,\beta_m}\gamma_{\omega,3}^{t},\\
\gamma\gamma_{17}(t) &= \gamma\gamma_{1,8}^{\lambda_m,\alpha,\beta_m}\gamma_{\omega,5}^{t} - \gamma\gamma_{1,6}^{\lambda_m,\alpha,\beta_m}\gamma_{\omega,6}^{t},\\
\gamma\gamma_{18}(t) &= \gamma\gamma_{1,8}^{\lambda_m,\alpha,\beta_m}\gamma_{\omega,6}^{t} - \gamma\gamma_{1,6}^{\lambda_m,\alpha,\beta_m}\gamma_{\omega,5}^{t},\\
\gamma\gamma_{1,0}^{\lambda_m} &= \frac{1}{\lambda_m^5},\\
\gamma\gamma_{1,1}^{\lambda_m,\alpha,\beta_m} &= \frac{\alpha^2\left(\lambda_m^4 - \alpha^2\lambda_m^2 - 4\beta_m^2\right)}{\lambda_m^5\gamma d_1^{\lambda_m,\alpha,\beta_m}},\\
\gamma\gamma_{1,2}^{\lambda_m,\alpha,\beta_m} &= \frac{\alpha^2\left(\lambda_m^4 + \alpha^2\lambda_m^2 - 4\beta_m^2\right)}{\lambda_m^5\gamma d_2^{\lambda_m,\alpha,\beta_m}},\\
\gamma\gamma_{1,3}^{\lambda_m,\alpha,\beta_m} &= \frac{\alpha^2\beta_m\left(3\lambda_m^4 - \alpha^2\lambda_m^2 - 4\beta_m^2\right)}{\lambda_m^5\sqrt{\lambda_m^4 - \beta_m^2}\,\gamma d_1^{\lambda_m,\alpha,\beta_m}},\\
\gamma\gamma_{1,4}^{\lambda_m,\alpha,\beta_m} &= \frac{\alpha^2\beta_m\left(3\lambda_m^4 + \alpha^2\lambda_m^2 - 4\beta_m^2\right)}{\lambda_m^5\sqrt{\lambda_m^4 - \beta_m^2}\,\gamma d_2^{\lambda_m,\alpha,\beta_m}},\\
\gamma\gamma_{1,5}^{\lambda_m,\alpha,\beta_m} &= \frac{2\alpha^2\beta_m}{\lambda_m^2\gamma d_1^{\lambda_m,\alpha,\beta_m}},\\
\gamma\gamma_{1,6}^{\lambda_m,\alpha,\beta_m} &= \frac{2\alpha^2\beta_m}{\lambda_m^2\gamma d_2^{\lambda_m,\alpha,\beta_m}},\\
\gamma\gamma_{1,7}^{\lambda_m,\alpha,\beta_m} &= \frac{\lambda_m^2 - \alpha^2}{\lambda_m^2\gamma d_2^{\lambda_m,\alpha,\beta_m}},\\
\gamma\gamma_{1,8}^{\lambda_m,\alpha,\beta_m} &= \frac{\lambda_m^2 + \alpha^2}{\lambda_m^2\gamma d_2^{\lambda_m,\alpha,\beta_m}},\\
\gamma\gamma_{1,9}^{\lambda_m,\alpha,\beta_m} &= \frac{\lambda_m^3\gamma\gamma_{1,1}^{\lambda_m,\alpha,\beta_m} + \alpha\beta_m\gamma\gamma_{1,5}^{\lambda_m,\alpha,\beta_m}}{\alpha\sqrt{\lambda_m^4 - \beta_m^2}},\\
\gamma\gamma_{1,10}^{\lambda_m,\alpha,\beta_m} &= \frac{\lambda_m^3\gamma\gamma_{1,2}^{\lambda_m,\alpha,\beta_m} + \alpha\beta_m\gamma\gamma_{1,6}^{\lambda_m,\alpha,\beta_m}}{\alpha\sqrt{\lambda_m^4 - \beta_m^2}},\\
\gamma d_1^{\lambda_m,\alpha,\beta_m} &= \lambda_m^2\left(\lambda_m^2 - \alpha^2\right)^2 + 4\alpha^2\beta_m^2,\\
\gamma d_2^{\lambda_m,\alpha,\beta_m} &= \lambda_m^2\left(\lambda_m^2 + \alpha^2\right)^2 - 4\alpha^2\beta_m^2,\\
\gamma_{\omega,1}^{t} &= \cos(\omega_D^m t)\exp(-\beta_m\omega_1 t),\\
\gamma_{\omega,2}^{t} &= \sin(\omega_D^m t)\exp(-\beta_m\omega_1 t).
\end{aligned}
\tag{B.11}
$$

C. Parameters of $\widehat{\Gamma}_{2nm}$ and $\breve{\Gamma}_{2nm}$

$$\widehat{\Gamma}_{2nm}(t) = [\,\widehat{\gamma}_{2nm1}\ \ \widehat{\gamma}_{2nm2}\ \ \widehat{\gamma}_{2nm3}\ \ \widehat{\gamma}_{2nm4}\,], \tag{C.1}$$

$$\breve{\Gamma}_{2nm}(t) = [\,\breve{\gamma}_{2nm1}\ \ \breve{\gamma}_{2nm2}\ \ \breve{\gamma}_{2nm3}\ \ \breve{\gamma}_{2nm4}\,], \tag{C.2}$$

$$\widehat{\gamma}_{2nm1} = \frac{\gamma\gamma_{21}(t) - \gamma\gamma_{25}(t)}{\lambda_m^2 - Q_n^2}, \tag{C.3}$$

$$\widehat{\gamma}_{2nm2} = \frac{\gamma\gamma_{22}(t) + \gamma\gamma_{26}(t)}{\lambda_m^2 - Q_n^2}, \tag{C.4}$$

$$\widehat{\gamma}_{2nm3} = \frac{\gamma\gamma_{23}(t) + \gamma\gamma_{27}(t)}{\lambda_m^2 + Q_n^2}, \tag{C.5}$$

$$\widehat{\gamma}_{2nm4} = \frac{\gamma\gamma_{24}(t) + \gamma\gamma_{28}(t)}{\lambda_m^2 + Q_n^2}, \tag{C.6}$$

$$\breve{\gamma}_{2nm1} = \frac{\gamma\gamma_{21}(t) - \gamma\gamma_{21}(t-t_1)\cos(\lambda_m\xi_1 L)}{\lambda_m^2 - Q_n^2} - \frac{\gamma\gamma_{22}(t-t_1)\sin(\lambda_m\xi_1 L)}{\lambda_m^2 - Q_n^2}, \tag{C.7}$$

$$\breve{\gamma}_{2nm2} = \frac{\gamma\gamma_{22}(t) - \gamma\gamma_{22}(t-t_1)\cos(\lambda_m\xi_1 L)}{\lambda_m^2 - Q_n^2} + \frac{\gamma\gamma_{21}(t-t_1)\sin(\lambda_m\xi_1 L)}{\lambda_m^2 - Q_n^2}, \tag{C.8}$$

$$\breve{\gamma}_{2nm3} = \frac{\gamma\gamma_{23}(t) - \gamma\gamma_{23}(t-t_1)\cosh(\lambda_m\xi_1 L)}{\lambda_m^2 + Q_n^2} - \frac{\gamma\gamma_{24}(t-t_1)\sinh(\lambda_m\xi_1 L)}{\lambda_m^2 + Q_n^2}, \tag{C.9}$$

$$\breve{\gamma}_{2nm4} = \frac{\gamma\gamma_{24}(t) - \gamma\gamma_{24}(t-t_1)\cosh(\lambda_m\xi_1 L)}{\lambda_m^2 + Q_n^2} - \frac{\gamma\gamma_{23}(t-t_1)\sinh(\lambda_m\xi_1 L)}{\lambda_m^2 + Q_n^2}, \tag{C.10}$$

where

$$\gamma\gamma_{21}(t) = \lambda_m\gamma\gamma_{2,1}^{\lambda_m,Q_n,\alpha,\beta_m}\gamma_{\omega,7}^{t} + \lambda_m\gamma\gamma_{2,2}^{\lambda_m,Q_n,\alpha,\beta_m}\gamma_{\omega,8}^{t} - \gamma\gamma_{2,3}^{\lambda_m,Q_n,\alpha,\beta_m}\gamma_{\omega,1}^{t} - \gamma\gamma_{2,5}^{\lambda_m,Q_n,\alpha,\beta_m}\gamma_{\omega,2}^{t},$$

$$\gamma\gamma_{22}(t) = Q_n\gamma\gamma_{2,2}^{\lambda_m,Q_n,\alpha,\beta_m}\gamma_{\omega,7}^{t} - Q_n\gamma\gamma_{2,1}^{\lambda_m,Q_n,\alpha,\beta_m}\gamma_{\omega,8}^{t} + \gamma\gamma_{2,7}^{\lambda_m,Q_n,\alpha,\beta_m}\gamma_{\omega,1}^{t} + \gamma\gamma_{2,9}^{\lambda_m,Q_n,\alpha,\beta_m}\gamma_{\omega,2}^{t},$$

$$\gamma\gamma_{23}(t) = -\lambda_m\gamma\gamma_{2,1}^{\lambda_m,Q_n,\alpha,\beta_m}\gamma_{\omega,7}^{t} - \lambda_m\gamma\gamma_{2,2}^{\lambda_m,Q_n,\alpha,\beta_m}\gamma_{\omega,8}^{t} - \gamma\gamma_{2,4}^{\lambda_m,Q_n,\alpha,\beta_m}\gamma_{\omega,1}^{t} - \gamma\gamma_{2,6}^{\lambda_m,Q_n,\alpha,\beta_m}\gamma_{\omega,2}^{t},$$

$$\gamma\gamma_{24}(t) = -Q_n\gamma\gamma_{2,2}^{\lambda_m,Q_n,\alpha,\beta_m}\gamma_{\omega,7}^{t} + Q_n\gamma\gamma_{2,1}^{\lambda_m,Q_n,\alpha,\beta_m}\gamma_{\omega,8}^{t} + \gamma\gamma_{2,8}^{\lambda_m,Q_n,\alpha,\beta_m}\gamma_{\omega,1}^{t} + \gamma\gamma_{2,10}^{\lambda_m,Q_n,\alpha,\beta_m}\gamma_{\omega,2}^{t},$$

$$\gamma\gamma_{25}(t) = \lambda_m^2\gamma\gamma_{15}(t),$$

$$\gamma\gamma_{26}(t) = \lambda_m^2\gamma\gamma_{16}(t),$$

$$\gamma\gamma_{27}(t) = \lambda_m^2\gamma\gamma_{17}(t),$$

$$\gamma\gamma_{28}(t) = \lambda_m^2\gamma\gamma_{18}(t),$$

$$\gamma\gamma_{2,1}^{\lambda_m,Q_n,\alpha,\beta_m} = \frac{\lambda_m^4 - \alpha^2 Q_n^2}{\gamma d_3^{\lambda_m,Q_n,\alpha,\beta_m}},$$

$$
\begin{aligned}
\gamma\gamma_{2,2}^{\lambda_m,Q_n,\alpha,\beta_m} &= \frac{2\alpha\beta_m Q_n}{\gamma d_3^{\lambda_m,Q_n,\alpha,\beta_m}},\\
\gamma\gamma_{2,3}^{\lambda_m,Q_n,\alpha,\beta_m} &= \alpha^2\lambda_m\left(\lambda_m^2 - Q_n^2\right)\frac{4\beta_m^2\lambda_m^2 - \left(\lambda_m^2 - \alpha^2 Q_n^2\right)\left(\lambda_m^2 - \alpha^2\right)}{\gamma d_1^{\lambda_m,\alpha,\beta_m}\gamma d_3^{\lambda_m,Q_n,\alpha,\beta_m}},\\
\gamma\gamma_{2,4}^{\lambda_m,Q_n,\alpha,\beta_m} &= \alpha^2\lambda_m\left(\lambda_m^2 + Q_n^2\right)\frac{4\beta_m^2\lambda_m^2 - \left(\lambda_m^2 - \alpha^2 Q_n^2\right)\left(\lambda_m^2 + \alpha^2\right)}{\gamma d_2^{\lambda_m,\alpha,\beta_m}\gamma d_3^{\lambda_m,Q_n,\alpha,\beta_m}},\\
\gamma\gamma_{2,5}^{\lambda_m,Q_n,\alpha,\beta_m} &= \frac{\alpha^2\lambda_m\left(\lambda_m^2 - Q_n^2\right)\beta_m}{\sqrt{\lambda_m^4 - \beta_m^2}}\,\frac{4\beta_m^2\lambda_m^2 + \left(\lambda_m^2 + \alpha^2 Q_n^2\right)\left(\lambda_m^2 + \alpha^2\right) - 4\lambda_m^6}{\gamma d_1^{\lambda_m,\alpha,\beta_m}\gamma d_3^{\lambda_m,Q_n,\alpha,\beta_m}},\\
\gamma\gamma_{2,6}^{\lambda_m,Q_n,\alpha,\beta_m} &= \frac{\alpha^2\lambda_m\left(\lambda_m^2 + Q_n^2\right)\beta_m}{\sqrt{\lambda_m^4 - \beta_m^2}}\,\frac{4\beta_m^2\lambda_m^2 + \left(\lambda_m^2 + \alpha^2 Q_n^2\right)\left(\lambda_m^2 - \alpha^2\right) - 4\lambda_m^6}{\gamma d_2^{\lambda_m,\alpha,\beta_m}\gamma d_3^{\lambda_m,Q_n,\alpha,\beta_m}},\\
\gamma\gamma_{2,7}^{\lambda_m,Q_n,\alpha,\beta_m} &= \alpha\left(\lambda_m^2 - Q_n^2\right)\frac{2\beta_m\left(\lambda_m^6 - \alpha^4 Q_n^2\right)}{\gamma d_1^{\lambda_m,\alpha,\beta_m}\gamma d_3^{\lambda_m,Q_n,\alpha,\beta_m}},\\
\gamma\gamma_{2,8}^{\lambda_m,Q_n,\alpha,\beta_m} &= \alpha\left(\lambda_m^2 + Q_n^2\right)\frac{2\beta_m\left(\lambda_m^6 + \alpha^4 Q_n^2\right)}{\gamma d_2^{\lambda_m,\alpha,\beta_m}\gamma d_3^{\lambda_m,Q_n,\alpha,\beta_m}},\\
\gamma\gamma_{2,9}^{\lambda_m,Q_n,\alpha,\beta_m} &= \frac{\lambda_m^3\gamma\gamma_{2,3}^{\lambda_m,Q_n,\alpha,\beta_m} - \alpha\beta_m\gamma\gamma_{2,7}^{\lambda_m,Q_n,\alpha,\beta_m}}{\alpha\sqrt{\lambda_m^4 - \beta_m^2}},\\
\gamma\gamma_{2,10}^{\lambda_m,Q_n,\alpha,\beta_m} &= \frac{\lambda_m^3\gamma\gamma_{2,4}^{\lambda_m,Q_n,\alpha,\beta_m} - \alpha\beta_m\gamma\gamma_{2,8}^{\lambda_m,Q_n,\alpha,\beta_m}}{\alpha\sqrt{\lambda_m^4 - \beta_m^2}},\\
\gamma d_3^{\lambda_m,Q_n,\alpha,\beta_m} &= \left(\lambda_m^4 - \alpha^2 Q_n^2\right)^2 + 4\alpha^2\beta_m^2 Q_n^2.
\end{aligned}
\tag{C.11}
$$

D. Parameters of $\widehat{\Gamma}_{3nm}$ and $\breve{\Gamma}_{3nm}$

$$\widehat{\Gamma}_{3nm}(t) = \left[\,\widehat{\gamma}_{3nm1}\quad \widehat{\gamma}_{3nm2}\quad \widehat{\gamma}_{3nm3}\quad \widehat{\gamma}_{3nm4}\,\right], \tag{D.1}$$

$$\breve{\Gamma}_{3nm}(t) = \left[\,\breve{\gamma}_{3nm1}\quad \breve{\gamma}_{3nm2}\quad \breve{\gamma}_{3nm3}\quad \breve{\gamma}_{3nm4}\,\right], \tag{D.2}$$

$$\widehat{\gamma}_{3nm1} = \frac{\gamma\gamma_{31}(t) - \gamma\gamma_{35}(t)}{\lambda_m^2 - Q_n^2}, \tag{D.3}$$

$$\widehat{\gamma}_{3nm2} = \frac{\gamma\gamma_{32}(t) + \gamma\gamma_{36}(t)}{\lambda_m^2 - Q_n^2}, \tag{D.4}$$

$$\widehat{\gamma}_{3nm3} = \frac{\gamma\gamma_{33}(t) + \gamma\gamma_{37}(t)}{\lambda_m^2 + Q_n^2}, \tag{D.5}$$

$$\widehat{\gamma}_{3nm4} = \frac{\gamma\gamma_{34}(t) + \gamma\gamma_{38}(t)}{\lambda_m^2 + Q_n^2}, \tag{D.6}$$

$$\breve{\gamma}_{3nm1} = \frac{\gamma\gamma_{31}(t) - \gamma\gamma_{31}(t - t_1)\cos(\lambda_m\xi_1 L)}{\lambda_m^2 - Q_n^2} - \frac{\gamma\gamma_{32}(t - t_1)\sin(\lambda_m\xi_1 L)}{\lambda_m^2 - Q_n^2}, \tag{D.7}$$

$$\breve{\gamma}_{3nm2} = \frac{\gamma\gamma_{32}(t) - \gamma\gamma_{32}(t-t_1)\cos(\lambda_m\xi_1 L)}{\lambda_m^2 - Q_n^2} + \frac{\gamma\gamma_{31}(t-t_1)\sin(\lambda_m\xi_1 L)}{\lambda_m^2 - Q_n^2}, \tag{D.8}$$

$$\breve{\gamma}_{3nm3} = \frac{\gamma\gamma_{33}(t) - \gamma\gamma_{23}(t-t_1)\cosh(\lambda_m\xi_1 L)}{\lambda_m^2 + Q_n^2} - \frac{\gamma\gamma_{34}(t-t_1)\sinh(\lambda_m\xi_1 L)}{\lambda_m^2 + Q_n^2}, \tag{D.9}$$

$$\breve{\gamma}_{3nm4} = \frac{\gamma\gamma_{34}(t) - \gamma\gamma_{34}(t-t_1)\cosh(\lambda_m\xi_1 L)}{\lambda_m^2 + Q_n^2} - \frac{\gamma\gamma_{33}(t-t_1)\sinh(\lambda_m\xi_1 L)}{\lambda_m^2 + Q_n^2}, \tag{D.10}$$

where

$$\begin{aligned}
\gamma\gamma_{31}(t) &= \lambda_m\gamma\gamma_{3,2}^{\lambda_m,Q_n,\alpha,\beta_m}\gamma_{\omega,7}^{t} - \lambda_m\gamma\gamma_{3,1}^{\lambda_m,Q_n,\alpha,\beta_m}\gamma_{\omega,8}^{t} \\
&\quad - \gamma\gamma_{3,7}^{\lambda_m,Q_n,\alpha,\beta_m}\gamma_{\omega,1}^{t} - \gamma\gamma_{3,9}^{\lambda_m,Q_n,\alpha,\beta_m}\gamma_{\omega,2}^{t}, \\
\gamma\gamma_{32}(t) &= -Q_n\gamma\gamma_{3,1}^{\lambda_m,Q_n,\alpha,\beta_m}\gamma_{\omega,7}^{t} - Q_n\gamma\gamma_{3,2}^{\lambda_m,Q_n,\alpha,\beta_m}\gamma_{\omega,8}^{t} \\
&\quad + \gamma\gamma_{3,3}^{\lambda_m,Q_n,\alpha,\beta_m}\gamma_{\omega,1}^{t} + \gamma\gamma_{3,5}^{\lambda_m,Q_n,\alpha,\beta_m}\gamma_{\omega,2}^{t}, \\
\gamma\gamma_{33}(t) &= -\lambda_m\gamma\gamma_{3,2}^{\lambda_m,Q_n,\alpha,\beta_m}\gamma_{\omega,7}^{t} + \lambda_m\gamma\gamma_{3,1}^{\lambda_m,Q_n,\alpha,\beta_m}\gamma_{\omega,8}^{t} \\
&\quad - \gamma\gamma_{3,8}^{\lambda_m,Q_n,\alpha,\beta_m}\gamma_{\omega,1}^{t} - \gamma\gamma_{3,10}^{\lambda_m,Q_n,\alpha,\beta_m}\gamma_{\omega,2}^{t}, \\
\gamma\gamma_{34}(t) &= Q_n\gamma\gamma_{3,1}^{\lambda_m,Q_n,\alpha,\beta_m}\gamma_{\omega,7}^{t} + Q_n\gamma\gamma_{3,2}^{\lambda_m,Q_n,\alpha,\beta_m}\gamma_{\omega,8}^{t} \\
&\quad + \gamma\gamma_{3,4}^{\lambda_m,Q_n,\alpha,\beta_m}\gamma_{\omega,1}^{t} + \gamma\gamma_{3,6}^{\lambda_m,Q_n,\alpha,\beta_m}\gamma_{\omega,2}^{t}, \\
\gamma\gamma_{35}(t) &= \lambda_m Q_n\left(\gamma\gamma_{1,5}^{\lambda_m,\alpha,\beta_m}\gamma_{\omega,3}^{t} - \gamma\gamma_{1,7}^{\lambda_m,\alpha,\beta_m}\gamma_{\omega,4}^{t}\right), \\
\gamma\gamma_{36}(t) &= \lambda_m Q_n\left(\gamma\gamma_{1,7}^{\lambda_m,\alpha,\beta_m}\gamma_{\omega,3}^{t} + \gamma\gamma_{1,5}^{\lambda_m,\alpha,\beta_m}\gamma_{\omega,4}^{t}\right), \\
\gamma\gamma_{37}(t) &= \lambda_m Q_n\left(\gamma\gamma_{1,6}^{\lambda_m,\alpha,\beta_m}\gamma_{\omega,5}^{t} - \gamma\gamma_{1,8}^{\lambda_m,\alpha,\beta_m}\gamma_{\omega,6}^{t}\right), \\
\gamma\gamma_{38}(t) &= \lambda_m Q_n\left(-\gamma\gamma_{1,8}^{\lambda_m,\alpha,\beta_m}\gamma_{\omega,5}^{t} + \gamma\gamma_{1,6}^{\lambda_m,\alpha,\beta_m}\gamma_{\omega,6}^{t}\right), \\
\gamma\gamma_{3,1}^{\lambda_m,Q_n,\alpha,\beta_m} &= \gamma\gamma_{2,1}^{\lambda_m,Q_n,\alpha,\beta_m}, \\
\gamma\gamma_{3,2}^{\lambda_m,Q_n,\alpha,\beta_m} &= \gamma\gamma_{2,2}^{\lambda_m,Q_n,\alpha,\beta_m}, \\
\gamma\gamma_{3,3}^{\lambda_m,Q_n,\alpha,\beta_m} &= \frac{Q_n}{\lambda_m}\gamma\gamma_{2,3}^{\lambda_m,Q_n,\alpha,\beta_m}, \\
\gamma\gamma_{3,4}^{\lambda_m,Q_n,\alpha,\beta_m} &= \frac{Q_n}{\lambda_m}\gamma\gamma_{2,4}^{\lambda_m,Q_n,\alpha,\beta_m}, \\
\gamma\gamma_{3,5}^{\lambda_m,Q_n,\alpha,\beta_m} &= \frac{Q_n}{\lambda_m}\gamma\gamma_{2,5}^{\lambda_m,Q_n,\alpha,\beta_m}, \\
\gamma\gamma_{3,6}^{\lambda_m,Q_n,\alpha,\beta_m} &= \frac{Q_n}{\lambda_m}\gamma\gamma_{2,6}^{\lambda_m,Q_n,\alpha,\beta_m},
\end{aligned}$$

$$\begin{aligned}
\gamma\gamma_{3,7}^{\lambda_m,Q_n,\alpha,\beta_m} &= \frac{\alpha^3 Q_n\left(\lambda_m^2 - Q_n^2\right)}{\lambda_m}\frac{2\beta_m\left(\alpha^2 Q_n^2 + 4\beta_m^2 + \alpha^2\lambda_m^2 - 2\lambda_m^4\right)}{\gamma d_1^{\lambda_m,\alpha,\beta_m}\gamma d_3^{\lambda_m,Q_n,\alpha,\beta_m}},\\
\gamma\gamma_{3,8}^{\lambda_m,Q_n,\alpha,\beta_m} &= \frac{\alpha^3 Q_n\left(\lambda_m^2 + Q_n^2\right)}{\lambda_m}\frac{2\beta_m\left(\alpha^2 Q_n^2 + 4\beta_m^2 - \alpha^2\lambda_m^2 - 2\lambda_m^4\right)}{\gamma d_2^{\lambda_m,\alpha,\beta_m}\gamma d_3^{\lambda_m,Q_n,\alpha,\beta_m}},\\
\gamma\gamma_{3,9}^{\lambda_m,Q_n,\alpha,\beta_m} &= \frac{\beta_m\gamma\gamma_{3,7}^{\lambda_m,Q_n,\alpha,\beta_m} - \alpha\lambda_m\gamma\gamma_{3,3}^{\lambda_m,Q_n,\alpha,\beta_m}}{\sqrt{\lambda_m^4 - \beta_m^2}},\\
\gamma\gamma_{3,10}^{\lambda_m,Q_n,\alpha,\beta_m} &= \frac{\beta_m\gamma\gamma_{3,8}^{\lambda_m,Q_n,\alpha,\beta_m} - \alpha\lambda_m\gamma\gamma_{3,4}^{\lambda_m,Q_n,\alpha,\beta_m}}{\sqrt{\lambda_m^4 - \beta_m^2}}.
\end{aligned} \tag{D.11}$$

E. Finite Element Procedure for Solving Moving Distributed Force Problem

Since the distributed force is a function of space moving at a certain speed, there is a complex procedure to calculate the equivalent force and moment vectors for all nodes on the beam at all time steps, which indeed limits the utilization of FEM to moving load problems. Until now, there is no reference for solving this problem by using FEM. In fact, FEM can give an approximate result of the moving distributed force problem by some special treatment of distributed force, element size, and time step, which is illustrated below:

(1) Mesh the beam (length is L) and the distributed force (length is $\widetilde{L}$) with equal element size ΔL. The total number of beam elements is $N = L/\Delta L$, and the number of force segments is $\widetilde{L}/\Delta L$.

(2) Substitute each segment of original force to trapezoidal distributed force. The new formed distributed force is called simplified force.

(3) Let the simplified force move on the beam at the speed v, and length of time step Δt equal to $\Delta L/v$.

(4) Calculate the vibration of the beam at each time step using dynamic finite element procedure as illustrated in Figure 16.

Data Availability

The dynamic air pressure acting upon the purlin due to the train passing and its corresponding acceleration were sampled in a filed test, which was located on the Beijing-Shanghai high-speed railway in China. Due to the restrictions of the contract, we cannot share our data in a repository. But the data used to support the findings of this study are available from the corresponding author upon request.

Conflicts of Interest

The authors declare that they have no conflicts of interest.

Acknowledgments

This work was supported by the National Natural Science Foundation of China (grant no. 51578349) and the Hebei Provincial Key Laboratory of Behavioral Evolution and Control of Structural Mechanics in Traffic Engineering (STKF201706).

References

[1] S. Timoshenko, *History of Strength of Materials: With a Brief Account of the History of Theory of Elasticity and Theory of Structures*, Dover Publications, Mineola, NY, USA, 1983.

[2] S. P. Timoshenko, "CV. On the forced vibrations of bridges," *The London, Edinburgh, and Dublin Philosophical Magazine and Journal of Science*, vol. 43, no. 257, pp. 1018-1019, 1922.

[3] M. Olsson, "On the fundamental moving load problem," *Journal of Sound and Vibration*, vol. 145, no. 2, pp. 299–307, 1991.

[4] A. V. Pesterev, B. Yang, L. A. Bergman, and C. A. Tan, "Revisiting the moving force problem," *Journal of Sound and Vibration*, vol. 261, no. 1, pp. 75–91, 2003.

[5] Y. B. Yang, C. L. Lin, J. D. Yau, and D. W. Chang, "Mechanism of resonance and cancellation for train-induced vibrations on bridges with elastic bearings," *Journal of Sound and Vibration*, vol. 269, no. 1-2, pp. 345–360, 2004.

[6] C. Inglis, *A Mathematical Treatise on Vibrations in Railway Bridges*, Cambridge at the University Press, Cambridge, UK, 1934.

[7] Y.-B. Yang, S.-S. Liao, and B.-H. Lin, "Impact formulas for vehicles moving over simple and continuous beams," *Journal of Structural Engineering*, vol. 121, no. 11, pp. 1644–1650, 1995.

[8] Y.-B. Yang, J.-D. Yau, and L.-C. Hsu, "Vibration of simple beams due to trains moving at high speeds," *Engineering Structures*, vol. 19, no. 11, pp. 936–944, 1997.

[9] J. Li and M. Su, "The resonant vibration for a simply supported girder bridge under high-speed trains," *Journal of Sound and Vibration*, vol. 224, no. 5, pp. 897–915, 1999.

[10] H. Xia, N. Zhang, and W. W. Guo, "Analysis of resonance mechanism and conditions of train-bridge system," *Journal of Sound and Vibration*, vol. 297, no. 3–5, pp. 810–822, 2006.

[11] C. Adam and P. Salcher, "Dynamic effect of high-speed trains on simple bridge structures," *Structural Engineering and Mechanics*, vol. 51, no. 4, pp. 581–599, 2014.

[12] P. Salcher and C. Adam, "Quick assessment of high-speed railway bridges based on a non-dimensional parameter

representation," *Advances in Structural Engineering*, vol. 20, no. 11, pp. 1623–1631, 2017.

[13] H. Ouyang, "Moving-load dynamic problems: a tutorial (with a brief overview)," *Mechanical Systems and Signal Processing*, vol. 25, no. 6, pp. 2039–2060, 2011.

[14] L. Frýba, *Vibration of Solids and Structures under Moving Loads*, Thomas Telford Ltd, London, UK, 1999.

[15] A. H. Karimi and S. Ziaei-Rad, "Vibration analysis of a beam with moving support subjected to a moving mass travelling with constant and variable speed," *Communications in Nonlinear Science and Numerical Simulation*, vol. 29, no. 1–3, pp. 372–390, 2015.

[16] Y. Pi and H. Ouyang, "Vibration control of beams subjected to a moving mass using a successively combined control method," *Applied Mathematical Modelling*, vol. 40, no. 5-6, pp. 4002–4015, 2016.

[17] K. Rajabi, M. H. Kargarnovin, and M. Gharini, "Dynamic analysis of a functionally graded simply supported Euler-Bernoulli beam subjected to a moving oscillator," *Acta Mechanica*, vol. 224, no. 2, pp. 425–446, 2013.

[18] M. Ebrahimi, S. Gholampour, H. Jafarian Kafshgarkolaei, and I. M. Nikbin, "Dynamic behavior of a multispan continuous beam traversed by a moving oscillator," *Acta Mechanica*, vol. 226, no. 12, pp. 4247–4257, 2015.

[19] J. S. Wu and C. W. Dai, "Dynamic responses of multispan nonuniform beam due to moving loads," *Journal of Structural Engineering*, vol. 113, no. 3, pp. 458–474, 1987.

[20] C. W. Cai, Y. K. Cheung, and H. C. Chan, "Dynamic response of infinite continuous beams subjected to a moving force-an exact method," *Journal of Sound and Vibration*, vol. 123, no. 3, pp. 461–472, 1988.

[21] X. Q. Zhu and S. S. Law, "Precise time-step integration for the dynamic response of a continuous beam under moving loads," *Journal of Sound and Vibration*, vol. 240, no. 5, pp. 962–970, 2001.

[22] Y. A. Dugush and M. Eisenberger, "Vibrations of non-uniform continuous beams under moving loads," *Journal of Sound and Vibration*, vol. 254, no. 5, pp. 911–926, 2002.

[23] A. E. Martinez-Castro, P. Museros, and A. Castillo-Linares, "Semi-analytic solution in the time domain for non-uniform multi-span Bernoulli-euler beams traversed by moving loads," *Journal of Sound and Vibration*, vol. 294, no. 1-2, pp. 278–297, 2006.

[24] V. D. Salvo, G. Muscolino, and A. Palmeri, "A substructure approach tailored to the dynamic analysis of multi-span continuous beams under moving loads," *Journal of Sound and Vibration*, vol. 329, no. 15, pp. 3101–3120, 2010.

[25] Y.-H. Lin and M. W. Trethewey, "Finite element analysis of elastic beams subjected to moving dynamic loads," *Journal of Sound and Vibration*, vol. 136, no. 2, pp. 323–342, 1990.

[26] J.-J. Wu, A. R. Whittaker, and M. P. Cartmell, "The use of finite element techniques for calculating the dynamic response of structures to moving loads," *Computers & Structures*, vol. 78, no. 6, pp. 789–799, 2000.

[27] K. Henchi, M. Fafard, G. Dhatt, and M. Talbot, "Dynamic behaviour of multi-span beams under moving loads," *Journal of Sound and Vibration*, vol. 199, no. 1, pp. 33–50, 1997.

[28] N. Azizi, M. M. Saadatpour, and M. Mahzoon, "Using spectral element method for analyzing continuous beams and bridges subjected to a moving load," *Applied Mathematical Modelling*, vol. 36, no. 8, pp. 3580–3592, 2012.

[29] Y. Song, T. Kim, and U. Lee, "Vibration of a beam subjected to a moving force: frequency-domain spectral element modeling and analysis," *International Journal of Mechanical Sciences*, vol. 113, pp. 162–174, 2016.

[30] T. Kim and U. Lee, "Dynamic analysis of a multi-span beam subjected to a moving force using the frequency domain spectral element method," *Computers & Structures*, vol. 192, pp. 181–195, 2017.

[31] E. Esmailzadeh and M. Ghorashi, "Vibration analysis of beams traversed by uniform partially distributed moving masses," *Journal of Sound and Vibration*, vol. 184, no. 1, pp. 9–17, 1995.

[32] E. Esmailzadeh and M. Ghorashi, "Vibration analysis of a timoshenko beam subjected to a travelling mass," *Journal of Sound and Vibration*, vol. 199, no. 4, pp. 615–628, 1997.

[33] P. Museros, M. L. Romero, A. Poy, and E. Alarcón, "Advances in the analysis of short span railway bridges for high-speed lines," *Computers & Structures*, vol. 80, no. 27–30, pp. 2121–2132, 2002.

[34] R. Rehnström and W. Daniel, "*The influence of ballast on the vibrations of railway bridges*," M.S. thesis, Royal Institute of Technology, Stockholm, Sweden, 2012.

[35] A. Erik, S. Annelie, Ü.-K. Mahir, and B. Jean-Marc, "Effect of axle load spreading and support stiffness on the dynamic response of short span railway bridges," *Structural Engineering International*, vol. 24, no. 4, pp. 457–465, 2014.

[36] Z. Jin, B. Huang, J. Ren, and S. Pei, "Reduction of vehicle-induced vibration of railway bridges due to distribution of axle loads through track," *Shock and Vibration*, vol. 2018, Article ID 2431980, 14 pages, 2018.

[37] R. W. Clough and J. Penzien, *Dynamics of Structures*, McGraw-Hill, New York, NY, USA, 1975.

[38] T. Gilbert, C. Baker, and A. Quinn, "Aerodynamic pressures around high-speed trains: the transition from unconfined to enclosed spaces," *Proceedings of the Institution of Mechanical Engineers, Part F: Journal of Rail and Rapid Transit*, vol. 227, no. 6, pp. 609–622, 2013.

[39] CEN European Standard, *Railway Applications—Aerodynamics—Part 4: Requirements and Test Procedures for Aerodynamics on Open Track*, CEN EN, Brussels, Belgium, 2013.

[40] China Railway Design Corporation, *Code for Design of High Speed Railway, TB 10621-2014*, China Railway Design Corporation, Tianjin, China, 2014.

[41] Y. Yang and W. Zhao, "Curvelet transform-based identification of void diseases in ballastless track by ground-penetrating radar," *Structural Control and Health Monitoring*, vol. 26, no. 4, 2019.

[42] C. Tomas, "A short tutorial on obtaining fourier series coefficients via fft," 2004, http://pages.mtu.edu/tbco/cm416/fft1.pdf.